Master's Thesis

An Investigation into the Interaction of Biomass Ash and K-Feldspar as Bed Material in Fluidized-Bed Combustion and Gasification

carried out for the purpose of obtaining the degree of Master of Science (MSc), submitted at TU Wien, Faculty of Mechanical and Industrial Engineering, by

Norbert MEDLITSCH

Mat.Nr.: 00625602

under the supervision of

Univ.Prof. Dipl.-Ing. Dr.techn. Hermann HOFBAUER
Institute of Chemical, Environmental & Biological Engineering

reviewed by

Hermann HOFBAUER
Institute of Chemical, Environmental & Biological Engineering
Getreidemarkt 9/166
A-1060 Vienna

Matthias KUBA
BIOENERGY 2020+ GmbH
Wienerstraße 49
A-7540 Güssing

Affidavit

I declare in lieu of oath, that I wrote this thesis and performed the associated research myself, using only literature cited in this volume. If text passages from sources are used literally, they are marked as such.
I confirm that this work is original and has not been submitted elsewhere for any examination, nor is it currently under consideration for a thesis elsewhere.

Vienna, June 2017 _____

Signature

Abstract

Increasing concentrations of greenhouse gases such as CO_2 in the atmosphere are driving a development towards technologies using renewable sources to provide for the global energy demand. Biomass plays a major role in the substitution of fossil fuels with renewable energy carriers. It constitutes a suitable feedstock for biomass gasification technologies in which biomass is converted into a secondary energy carrier, called product gas. Product gas can be used to generate electricity and chemical products such as hydrogen, Fischer-Tropsch diesel, or alcohols. Dual fluidized-bed gasification systems circulate the bed material olivine between two separate combustion and gasification units. Interaction of biomass ash and bed material causes the formation of calcium-rich layers on bed materials which provide catalytic activity towards tar reduction. A shift from more expensive bed materials such as olivine to low-cost bed materials such as K-feldspar could further improve the gasification process.

The empirical part of this study comprised three combustion experiments in a 5 kW bench-scale fluidized-bed reactor. Three pelletized fuel mixtures were combusted at 780-800 °C: Straw (100 % straw), Chicken Litter Low (CLH, 90 % straw, 10 % chicken litter), and Chicken Litter High (CLH, 70 % straw, 30 % chicken litter). 540 g of fresh potassium (K)-feldspar particles with a grain size between 200-250 µm were used as bed material. Bed samples were taken during combustion and after defluidization. The samples were analyzed with scanning electron microscopy (SEM) combined with energy-dispersive spectroscopy (EDS). Individual and layered element mappings were evaluated to determine qualitative layer formation during initial hours of operation. Additional quantitative line scans were used to establish the thickness and elemental distribution of the qualitative layers. The total elemental com-

position of the used K-feldspar particles was obtained with X-ray fluorescence (XRF) spectrometry.

The experiments showed that the combustion of Straw and CLL resulted in very little interaction between the produced biomass ash and the K-feldspar particles. The relatively low calcium (Ca) content of both fuel mixtures lead to significantly diminished layer formation over time. No layers were found on the bed particles. Conversely, the high potassium (K) and silicon (Si) content in the ashes made for the formation of low-melting K-silicate ash particles that adhered to the surface of the bed materials and caused faster bed agglomeration. The results from the combustion of CLH showed initial layer formation on the bed particles. The higher Ca content in CLH facilitated the formation of continuous Ca-layers as found with the qualitative element mappings. Phosphorus (P) from the biomass ash was also found in the Ca-layers. Additionally, the total elemental composition of the used K-feldspar bed material included the elements Ca, Al, P, S, and Mg which were part of the biomass ash composition of CLH. This led to the conclusion that the layer formation process on K-feldspar particles could be ash-related. Future experiments should aim for advanced layer formation on K-feldspar particles to gain further insights into the layer formation mechanism on K-feldspar.

Kurzfassung

Steigende Konzentrationen von Treibhausgasen wie CO_2 in der Atmosphäre treiben die Entwicklung von Technologien voran, die auf der Verwendung erneuerbarer Ressourcen basieren, um die globale Energienachfrage abzudecken. Biomasse spielt dabei eine entscheidende Rolle, um fossile Brennstoffe durch erneuerbare Sekundärenergieträger zu ersetzen. Sie ist ein geeigneter Rohstoff für die Vergasungstechnologie, mit der Biomasse in einen gasförmigen, erneuerbaren Sekundärenergieträger, auch genannt Produktgas, umgewandelt werden kann. Das erzeugte Produktgas kann weiter zur Stromerzeugung verwendet werden, oder für die Herstellung chemischer Produkte wie Wasserstoff, Fischer-Tropsch Diesel, oder Alkohole. Zweibett-Wirbelschicht-Vergasungssysteme verwenden Olivin als Bettmaterial, das zwischen zwei separaten Reaktoren im Kreis geführt wird. Die Interaktion von Biomasseasche und Bettmaterial führt zur Bildung calciumhaltiger Schichten auf dem Bettmaterial, die katalytisch wirksam sind hinsichtlich der Verringerung von Teeren. Ein Umschwenken von teuren Bettmaterialien wie Olivin zu kostengünstigeren wie Kaliumfeldspat würde den Vergasungsprozess weiter verbessern.

Die durchgeführten Versuche zu dieser Studie umfassten drei Verbrennungsversuche in einer 5 kW Laborwirbelschicht. Drei Brennstoffmischungen wurden bei Temperaturen um 780-800 °C verfeuert: Stroh (100 % Stroh), Hühnermist-gering (CLL, 90 % Stroh, 10 % Hühnermist), und Hühnermist-hoch (CLH, 70 % Stroh, 30 % Hühnermist). 540 g an frischem Kaliumfeldspat mit Korngrößen zwischen 200-250 µm wurde als Bettmaterial eingesetzt. Proben von Bettmaterial wurden während der Versuche und nach der Defluidisierung genommen. Diese wurden mittels Rasterelektronenmikroskopie (REM) in Kombination mit energiedispersiver Spektroskopie (EDS) untersucht. Einzelne und überlagerte Elementkarten wurden herangezogen, um ein qualitatives Schichtwachstum innerhalb der ersten Versuchsstun-

den bestimmen zu können. Zusätzliche quantitative Linienscans wurden ausgeführt, um Schichtdicke und Elementverteilung der qualitativen Schichten zu ermitteln. Die elementare Gesamtzusammensetzung der verwendeten Kaliumfeldspatpartikel wurde mittels Röntgenfluoreszenzanalyse festgestellt.

Die Ergebnisse zeigten, dass die Verbrennung von Stroh und CLL zu einer geringen Interaktion von Biomasseasche und Kaliumfeldspat führte. Der relativ niedrige Calciumgehalt beider Brennstoffmischungen führte zu erheblich reduziertem Schichtwachstum innerhalb der Versuchsdauer. Es wurden keine Schichten auf den Bettmaterialien festgestellt. Ein hoher Gehalt an Calcium und Silicium in der Asche führte jedoch zur Bildung niedrigschmelzender Kaliumsilikat-Aschepartikel die an der Bettmaterialoberfläche klebten und zu frühzeitiger Agglomeration führten. Die Resultate der Verbrennungsversuche zu CLH zeigten beginnendes Schichtwachstum auf dem Bettmaterial. Der höhere Calciumgehalt in CLH ermöglichte die Bildung kontinuierlicher Calciumschichten. Phosphor, von der Biomasseasche stammend, wurde ebenfalls in den Calciumschichten festgestellt. Die Analyse der elementaren Gesamtzusammensetzung des verwendeten Kaliumfeldspats zeigte die Elemente Ca, Al, P, S, und Mg, die ebenfalls Bestandteil der Asche von CLH waren. Dies führte zu der Schlussfolgerung, dass die Schichtenbildung auf Kaliumfeldspat möglicherweise Aschebedingt ist. Zukünftige Versuche sollten darauf abzielen, eine besser ausgebildete Schicht auf Kaliumfeldspat zu erzeugen, um tiefere Einblicke in den Mechanismus der Schichtbildung auf Kaliumfeldspat zu erhalten.

Acknowledgements

I would like to express my sincere and deepest gratitude towards everyone who has contributed to this work.

First and foremost, I thank Prof. Hermann Hofbauer for his intriguing lectures on fluidized-bed technology. His passion and fascination for fluidized-bed systems and biomass conversion technologies ignited in me the interest to pursue a master's thesis in those fields of research.

I would also like to thank Matthias Kuba for the continuous support and supervision of my thesis. The discussions with him always gave me valuable insights and pointers during times of struggle and lack of clarity.

I appreciate the help of Juraj Priscak for the preparation of the fuel pellets before the experiments.

Special gratitude also goes out to my research colleagues from the University of Umeå and the Luleå University of Technology in Sweden. I had the opportunity to work closely with Nils Skoglund, Gustav Häggström, and Hanbing He during my monthly stay in Umeå in October 2016. Thank you for the explanations and discussions at the beginning of my study which helped me to get up to speed on the current research pertinent to this thesis. I would also like to thank all the other people I had the pleasure of meeting during the lunch breaks and occasional coffee conversations.

Most importantly, I would like to express my heartfelt gratitude towards my parents Elisabeth and Rudolf. I want them to know that their long-lasting support over the years is not taken for granted and that only their constant support made the completion of the master's thesis

possible in the first place. Furthermore, I want to thank my sister, Pia, for her encouraging and motivational words at times of difficulty before certain exams. Last but not least, I am lucky to have such a wonderful girlfriend, Ines, who supported me throughout our relationship and gave me the strength to overcome other hurdles in life as well. This was not an easy task bearing in mind that we managed to pull off a long-distance relationship. Thank you for your patience, Princess.

Contents

List of Figures

List of Tables

1 Introduction

Background

The awareness of increasing concentrations of greenhouse gases such as carbon dioxide (CO_2) and methane (CH_4) in the atmosphere has triggered a development towards technologies using renewable sources to cover the global energy demand. As a result, increasing efforts are undertaken to substitute fossil fuels with renewable energy carriers. Biomass is a viable renewable source as it is a carbon-based fuel and considered CO_2-neutral. It is suitable for conversion processes such as pyrolysis, combustion, and gasification. Gasification is an essential technology to convert the solid biomass feedstock into a gaseous secondary energy carrier, also called product gas or synthesis gas. The generated synthesis gas can further be used to produce district heat, electricity, as well as chemical products such as hydrogen, methane, Fischer-Tropsch diesel, or mixed alcohols.

A dual fluidized-bed gasification system has been developed at TU Wien, Austria. The key principle of this technology is the separation of gasification and combustion through the use of two separated reactor units. A bed material is circulating between the two reactors which functions as a heat carrier and a catalyst in the process. The prevalent bed material implemented nowadays is olivine. It provides good agglomeration performance and its catalytic activity facilitates tar reduction. However, interaction of biomass ash and bed material leads to the formation of calcium-rich layers on the olivine particles. Similar formations of Ca-rich layers were also observed on other bed materials such as quartz sand. The calcium-rich layers were found to significantly increase the activity for both olivine and quartz. Hence, the interaction of biomass ash and bed material can develop Ca-rich layers on variable bed materials with similar catalytic activity as olivine. The original catalytic activity will be replaced

by the catalytic effect of the formed layer.

Aim and structure

The aim of this study is to examine whether potassium (K) feldspar can be used as an alternative bed material regarding the ability to form Ca-rich layers during the interaction with biomass ash from fuel mixtures containing agricultural residues such as wheat straw and chicken litter. The experiments provide first insights into the layer formation mechanisms on K-feldspar bed particles. The literature review explores the background and fundamentals of combustion and gasification technologies and illustrates the similarities and differences. It elaborates on bed materials implemented in fluidized-bed systems and describes various biomass fuels. It expands on the composition and behavior of biomass ash in fluidized-bed systems and explains the identified layer formation mechanisms on different bed materials. The three bench-scale fluidized-bed combustion experiments, which were carried out at the University of Umeå, Sweden, are described in detail. This is followed by the presentation and discussion of the results. Finally, the conclusion points out the key findings and gives recommendations for further research.

2 Background and Fundamentals

2.1 Principles of biomass gasification and combustion

Gasification and combustion of biomass are two related thermo-chemical processes. Gasification focuses on the conversion of biomass into the so-called product gas, whereas combustion of biomass is mainly used to produce thermal energy. The principles as well as the basic similarities and differences of both processes are described in the following sections.

2.1.1 Gasification

The gasification process converts solid or liquid raw materials, e.g. biomass feedstock, into a product gas. The molecules in the yielded product gas store energy in their chemical bonds. This energy can be released by later combustion of the gas to generate thermal energy or utilized for the production of valuable chemical products (Basu, 2010, p.117). The generated product gas can therefore be described as a secondary energy carrier.

The gasification process requires the presence of a gasifying agent. Process temperatures in gasifiers of approximately 800-1400℃ are common. The temperatures allow for a reaction between the provided gasifying agents and the solid carbon atoms (C) in the feedstock structure to be converted into product gas.

Depending on the desired composition of the product gas, different gasifying agents and combinations can be chosen for the gasification. Currently, the more important gasifying agents comprise: oxygen (O_2), steam (H_2O), hydrogen (H_2), air (21 % O_2, 79 % N_2), and less frequently used, carbon dioxide (CO_2). The use of air as a gasifying agent introduces

the inert nitrogen gas (N_2) into the process, which results in a lower heating value for the product gas. The inert N_2 does not react with other constituents and only dilutes the product gas (Rosendahl, 2013, p.107).

The amount of oxygen or air in the gasification process is an important parameter. The air/fuel ratio (abbreviated λ) is the amout of air provided in the process divided by the amount of air theoretically required to achieve complete combustion. When oxygen or air is used as gasifying agent, incomplete combustion is favored in gasification. Incomplete combustion is the partial oxidation of organic matter from the fuel into carbon monoxide (CO) by the oxygen in the air, compared to carbon dioxide (CO_2) in complete combustion. The air/fuel ratio for gasification is between zero and one ($0 < \lambda < 1$) with typical values in the range of 0.2-0.4 for fluidized-bed gasification. The restricted amount of air for gasification leads to incomplete combustion, which generates more product gas. Introducing excess air would cause the generated product gas to be combusted. The use of steam as gasifying agent for the conversion process is often referred to as steam reforming.

Rosendahl (2013, p.107) states, the general composition of the product gas consists of main compounds, trace contaminants, a condensable fraction and particles. The main compounds include carbon monoxide (CO), hydrogen (H_2), methane (CH_4), lighter hydrocarbons (C2-C3), carbon dioxide (CO_2), steam (H_2O), and when air is used as gasifying agent, the inert nitrogen gas (N_2). Trace contaminants with nitrogen may comprise ammonia (NH_3) or hydrogen cyanide (HCN), and possible sulfur contaminants are hydrogen sulfide (H_2S) or carbonyl sulfide (COS), for example. The condensable fraction contains tar which is a highly viscous liquid condensing at low-temperature zones. Currently, there is no universally accepted definition for tar. Some suggestions refer to tar as the organic contaminants with a molecular weight larger than 78, which is the molecular weight for benzene. Particles can include ash, mineral matter/salts, char, or aerosols.

As mentioned before, gasification and combustion are two closely related thermo-chemical conversion processes. Therefore, subsection 2.1.2 describes the typical steps in the gasification process: drying, thermal decomposition or pyrolysis, and char gasification. Additionally, combustion is allowed in some gasification processes to generate the required energy

for heating, drying, pyrolysis and gasification.

The different types of gasifier configurations can be classified according to various aspects: the reactor type (gas-solid contacting mode), the energy supply (heat), the gasifying agent, the pressure conditions. Based on the reactor type or gas-solid interaction mode, gasifiers are generally divided into three principal groups: fixed-bed gasifiers (also called moving-bed gasifiers), fluidized-bed gasifiers, and entrained-flow gasifiers (Kaltschmitt et al., 2009, p.601), (Rosendahl, 2013, p.113).

The majority of reactions during gasification is of endothermic nature, meaning, they consume energy. The required energy for those reactions can be supplied in two ways: autothermal (internally) and allothermal (externally). The autothermal energy supply requires partial combustion of the biomass feedstock during gasification in the gasifier. Allothermal energy provision can be accomplished with a heat exchanger or by circulation of bed material as a heat carrier in a dual fluidized-bed gasifier (Kaltschmitt et al., 2009, p.395).

Fixed-bed gasification

In fixed-bed gasifiers the biomass feedstock is fed into the reactor from above and is supported by a grate near the bottom. This type is also called moving-bed gasifier, because the material slowly moves downward in the reactor due to gravitational force and continuing decomposition of the feedstock. As the decomposing material travels downward through the reactor, it passes through four spatial reaction zones: drying, pyrolysis, gasification, combustion. The fixed-bed gasifiers can be subdivided into three main groups: updraft gasifier, downdraft gasifier, and crossdraft gasifier. The distinguishing aspect is the relative movement of solid material and gas in the reactor (Basu, 2010, p.169).

Updraft gasifiers are counter-current gasifiers, as shown on the left in Figure 2.1. The gasifying agent enters at the bottom and flows upwards through the decomposing material. The product gas exits the reactor near the top. The solid feedstock progresses downwards, becomes gradually decomposed and the remaining ash leaves the reactor at the bottom.
Downdraft gasifiers are co-current gasifiers, as shown in the middle in Figure 2.1. The

decomposing biomass feedstock and the gasifying agent move into the same direction. As the gasifying agent enters the reactor at a certain height, it forms a combustion zone with the pyrolyzed char particles and continuous to descend through the hot char particles while gasifying them. Product gas and ash leave the reactor at the bottom.

Crossdraft gasifiers are co-current gasifiers with a modified configuration for gas inlet and outlet, as shown on the right in Figure 2.1. The decomposing biomass still progresses through the reactor from top to bottom with the ash collection on the lower end as well. The gasifying agent is introduced on one side of the reactor and forms a combustion zone with the char particles, immediately after injection. The hot gases further pass through the gasification zone, gasifying the hot char particles. Product gas leaves the reactor on the side opposite to the inlet point of the gasifying agent, hence, flowing through the reactor overall horizontally.

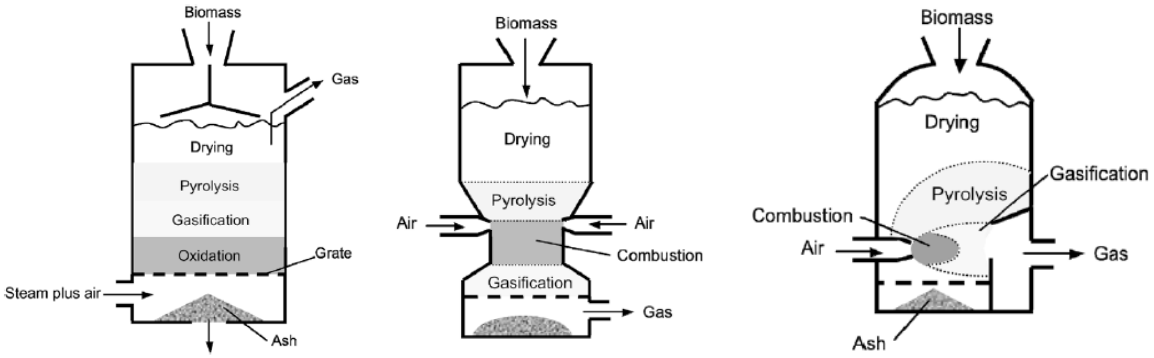

Figure 2.1: Schmematics of fixed-bed gasifiers from left to right: updraft gasifier, downdraft gasifier, crossdraft gasifier (Basu, 2010, p.171, p.173, p.176)

Fluidized-bed gasification

The minimum components for a fluidized bed comprise a container, fine granular solids, a fan, a gas distributor and a fluidizing medium. The fluidized bed is made of granular solids, called the bed material, which is suspended by the fluidizing medium passing through them. The right gas velocity for the fluidizing medium keeps the bed material in a fluidized state. Bed material is usually quartz sand, but can also be catalytically active minerals. The particle size of the feedstock for a fluidized-bed gasifier is generally smaller compared to a

fixed-bed gasifier. The intensive heat transfer from the bed material to the feedstock particles reduces the required residence time for the fuel feed in the reactor. Typically, the residence time for fuel particles ranges from seconds to minutes (Kaltschmitt et al., 2009, p.609).

The conditions in a fluidized bed support excellent gas-solid mixing and a uniform temperature distribution. As a consequence, the reaction steps for gasification occur simultaneously in fluidized-bed gasifiers. No discrete reaction zones or temperature zones are formed in the fluidized bed. The conditions also make the fluidized-bed gasifiers relatively insensitive to the quality of the fuel feedstock and considerably reduce the risk of bed agglomeration (Basu, 2010, p.177). In principle, three different main types of fluidized-bed gasifiers can be distinguished: bubbling fluidized-bed (BFB), circulating fluidized-bed (CFB), and dual fluidized-bed (DFB).

For bubbling fluidized-bed gasifiers the gas velocity of the fluidization medium is between the minimum fluidization velocity and the terminal velocity for one single particle of the bed material. Consequently, most of the bed material particles remain in the fluidized bed and only a small fraction of the bed material particles will be discharged (Kaltschmitt et al., 2009, p.611).

The particle diameter for bed material ranges from 500-1500 µm and the gas velocity is about 1-2 m/s. The size of the biomass feedstock can range from several millimeters up to 50 mm. The product gas leaves the gasification reactor at high temperatures, therefore, BFB gasifiers require internal heat recovery to obtain higher thermal efficiencies. Normally, BFB gasifiers are operated as autothermal gasifiers (Bridgewater et al., 2009, p.15).

In circulating fluidized-bed gasifiers the gas velocity is higher compared to bubbling fluidized-bed gasifiers. The gas velocity usually exceeds the terminal velocity for one individual particle of the fluidized bed. Therefore, the bed material particles are transported out of the fluidized-bed gasifier, called entrainment. The entrained particles are separated from the exiting product gas stream in a gas-solid separator, often in one or more cyclones. After separation, the bed particles are recirculated into the fluidized-bed gasifier, closing the circle for the bed material movement in CFB gasifiers.

The bed material particle diameter typically ranges from 250-500 µm combined with gas velocities of 5-10 m/s. These conditions create a fast fluidized bed which is expanded throughout the reactor. Indeed, the fluidized bed is not distributed evenly along the reactor. The lower section of the fluidized bed is denser than the top section. CFB gasifiers are normally operated as autothermal reactors (Bridgewater et al., 2009, p.15).

A dual fluidized-bed gasifier is a combination of two fluidized-bed configurations to generate a product gas with certain characteristics. The concept of a DFB gasification is shown in Figure 2.2. In a DFB gasifier, the gasification reactor is separated from the combustion reactor, but the two are connected to allow bed material circulation between them as depicted in Figure 2.3. The combustion system implements a fast fluidized-bed to generate heat by exothermic combustion of fuels. The heat from the combustor is transported to the gasification reactor by the circulating bed material which functions as a heat carrier. The gasification reactor is a bubbling fluidized-bed using steam as the gasifying medium. The required heat for the endothermic gasification reactions is provided by the circulating bed material from the combustor. Compared to BFB and CFB gasifiers, a DFB gasifier operates allothermical (Kaltschmitt et al., 2009, p.614).

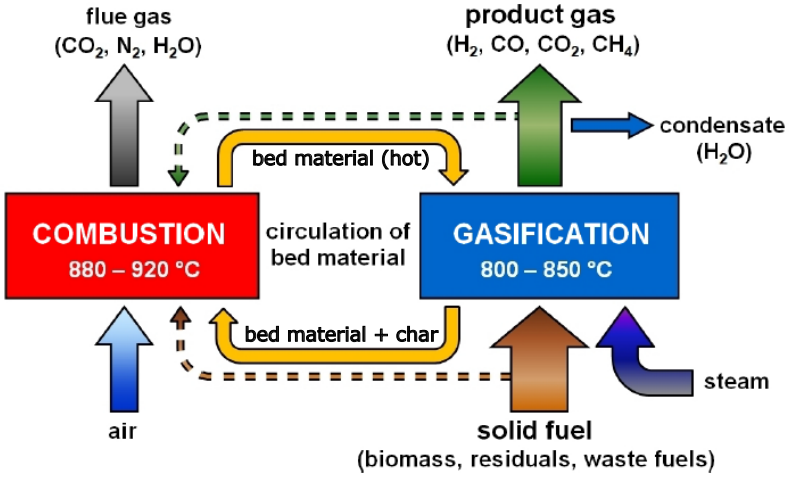

Figure 2.2: Concept of a dual fluidized-bed gasification process (Vienna University of Technology)

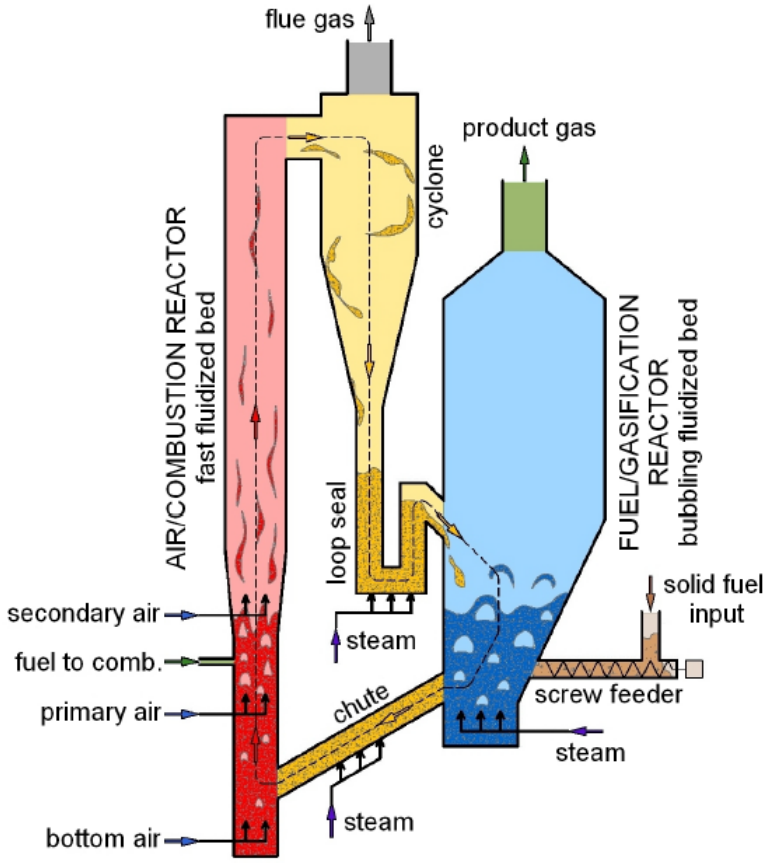

Figure 2.3: Gasifier design of a dual fluidized-bed gasification (designed by Vienna University of Technology)

Entrained-flow gasification

In entrained-flow gasifiers the conditioned feedstock is injected together with the gasifying medium at the top of the reactor. Therefore, the gasifiers are essentially co-current plug flow reactors, where gas and fuel progress into the same direction while nearly complete gasification occurs (Basu, 2010, p.186).

Figure 2.4 shows the basic layout of entrained-flow gasifiers for biomass. The very short residence time of a few seconds for particles and gas in the reactor requires extra preparation of the biomass. Very fine grinded biomass feedstock is produced and directly gasified in the reactor, or the biomass is pre-pyrolysed and the generated slurry (a mixture of pyrolysis oil and coke) is used as feed. The gasifying agent usually is a mixture of oxygen and steam. Process temperatures of over 1200 ℃ and local temperature maxima of up to

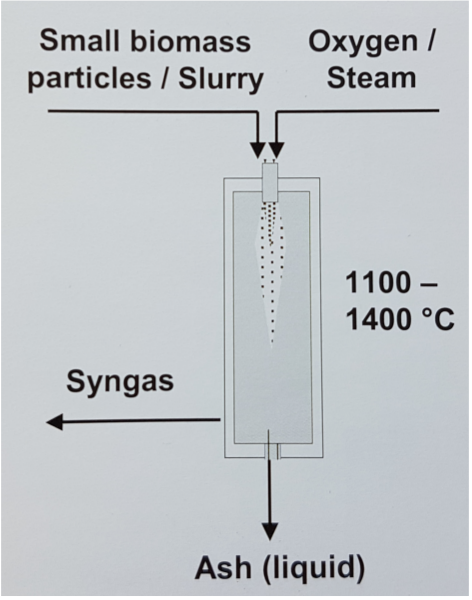

Figure 2.4: Basic layout of entrained-flow gasifiers for biomass (Bridgewater et al., 2009, p.17)

2500 ℃ put extra strain on the reactor and require elaborate technical effort to maintain and control those conditions. The high temperature also causes the ash to be in liquid form. Nowadays, entrained-flow gasifiers play an inferior role for biomass gasification due to the harsh process conditions and extra feed preparation. Therefore, entrained-flow gasifiers are more likely considered for plants with a high feedstock capacity (Kaltschmitt et al., 2009, p.617).

However, the process conditions allow the production of nearly tar-free product gas with very low methane content which is an advantage for downstream synthesis of liquid biofuels. Entrained-flow gasifiers have a high carbon conversion rate and pressurized operation is also possible (Basu, 2010, p.186). Generally, entrained-flow gasifiers can be subdivided into two main groups: top-fed gasifiers and side-fed gasifiers.

Top-fed gasifiers have a vertically cylindrical reactor vessel, as shown in Figure 2.5. Pulverized feedstock and the gasifying agent are injected with oxygen from the top and travel downwards. The design has resemblance to a vertical furnace with a downward burner usually situated in the reactor's middle section.

Side-fed gasifiers, as shown in Figure 2.6, inject fine fuel through horizontal nozzles ar-

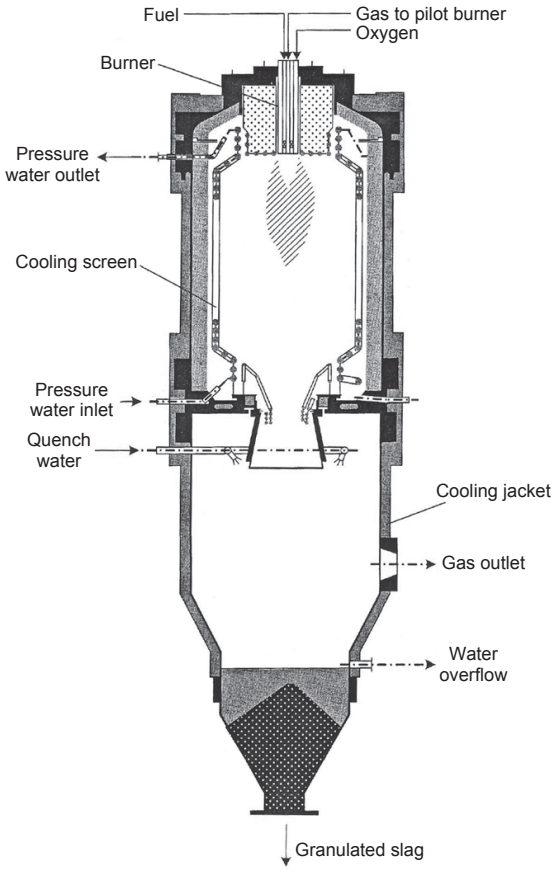

Figure 2.5: Schematic of top-fed downflow entrained-flow gasifier (Basu, 2010, p.188)

ranged opposite of each other in the lower section of the reactor. The introduced jets of fuel and gasifying agents form a stirred-tank reactor with excellent mixing behavior. The generated product gas travels upwards and leaves the reactor on the top. The high temperatures in the mixing zone cause the ash to melt and form slag. Contrary to the gas, the slag moves downwards and can be discharged at the bottom.

2.1.2 Combustion

The combustion process converts gaseous, liquid, or solid fuels, e.g biomass feedstock, into thermal energy. Compared to gasification, the stored energy in the chemical bonds of the fuel molecules is released by breaking those bonds during combustion (Basu, 2010, p.117). The generated thermal energy can be utilized as secondary energy carrier (steam

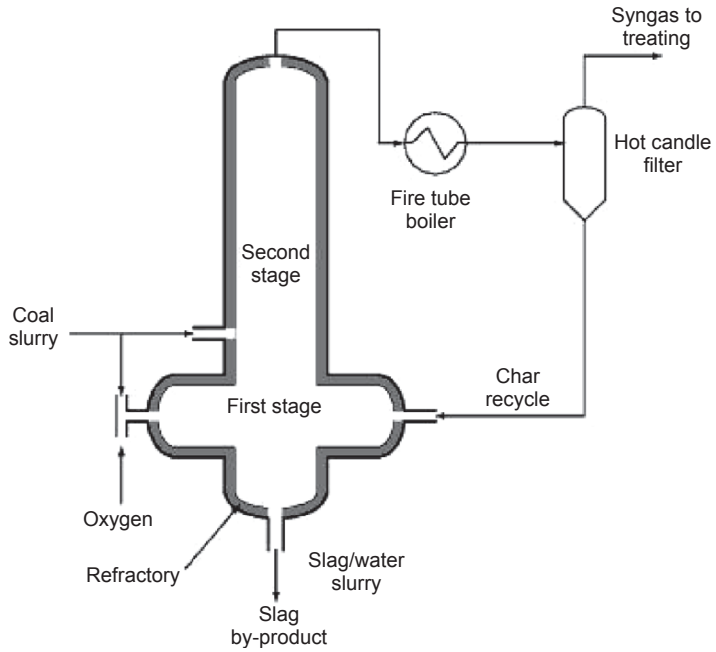

Figure 2.6: Schematic of side-fed entrained-flow gasifier (Basu, 2010, p.189)

production and subsequent conversion to electricity), useful energy (district heating), or final energy (Kaltschmitt et al., 2009, p.465).

Combustion requires the presence of an oxidizing agent to convert carbon (C) and hydrogen (H_2) to carbon dioxide (CO_2) and water (steam, H_2O). The oxidizing agent for combustion of biomass usually is oxygen (O_2) provided by air (21 % O_2, 79 % N_2). The oxidation process releases energy in the form of heat (thermal energy). Combustion usually takes place at temperatures of 700-1500 ℃ (Kaltschmitt et al., 2009, p.464).

The amount of oxygen or air used for the combustion is crucial for the quality of the combustion process. Combustion aims for the complete conversion of all organic constituents in the fuel, which is called complete combustion. To achieve that, the right amount of air needs to be introduced into the process. The amount of air is usually given in the air/fuel ratio, abbreviated with the greek letter λ. For combustion, the air/fuel ratio is greater than or equal to one ($\lambda \geq 1$) (Kaltschmitt et al., 2009, p.377). Typical values for λ are in the range of 1.2-1.4 for fluidized-bed combustion.

The combustion process of biomass typically comprises the following steps: drying, thermal

decomposition or pyrolysis, char gasification, and combustion. The steps do not necessarily occur consecutively, but also happen simultaneously and can overlap. Here, the steps are outlined for a single fuel particle.

Initially, the biomass feedstock particle is heated and dried. Starting at a temperature of about 100℃, the free moisture and some loosely bound water is evaporated. In the temperature range of 200-600℃ the thermal decomposition or pyrolysis takes place. Pyrolysis occurs in the absence of air or oxygen, and without an external reaction agent added. The products formed are condensable and noncondensable gas molecules, as well as char. Tar is formed through condensation of the condensable gas fraction at lower temperatures. The gasification step involves chemical reactions of hydrocarbons, steam, carbon dioxide, oxygen, hydrogen and the aforementioned pyrolysis products. The most important part is the gasification of char to carbon monoxide with carbon dioxide, hydrogen and oxygen. If gasification is the desired last process step, thus the production of product gas, reactions with the added gasifying agent also take place (see section 2.1.1 for details). On the other hand, if combustion is the main process goal, gasification still occurs, but the combustible gases are further oxidized to carbon dioxide and water. Complete combustion is the main objective to generate a maximum amount of thermal energy (Kaltschmitt et al., 2009, p.464). Combustion systems can be separated into three main groups with the type of gas-solid interaction as the classifying characteristic: fixed-bed combustion, fluidized-bed combustion, and entrained-flow combustion.

Fixed-bed combustion

Fixed-bed combustion systems have a grate where the fuel is fed on to from various sides. The necessary air for combustion is usually split into primary and secondary air. The primary air is supplied from below the grate and flows through the layer of fuel on the grate where drying, pyrolysis, gasification and combustion take place. Secondary air is typically introduced above the burning fuel bed where most of the generated combustible gases are further burned for complete combustion. Generally, there are two eminent fixed-bed combustion systems: grate furnaces and underfeed stokers (Lackner, 2010, p.121).

Grate furnace systems incorporate various designs of grate technologies: fixed grates, moving grates, traveling grates, rotating grates, and vibrating grates. The different types of grates bring the advantage of flexibility for grate furnaces. They are suitable for fuels with high moisture and ash content, as well as varying sizes of the fuel feedstock. Important is a uniform distribution of the fuel on the grate to ensure stable und homogeneous combustion conditions. Additionally, a continuous and steady transport of the fuel over the grate is mandatory to avoid the formation of hot-spots or gaps in the fuel layer. The grate structure is very important to accommodate different fuel properties. The grates itself can be oriented horizontally or inclined, and can be moving and/or fixed as well (Lackner, 2010, p.122).

In underfeed stokers the fuel feedstock is transported into the combustion chamber by screw conveyors from below and is further routed upwards on to a grate. The grates can be realized as inner or outer grates, however, outer grates are particularly used as they support more flexible operation and automatic ash removing. Primary air is typically introduced through the grate and the secondary air is supplied to a secondary combustion chamber for complete combustion of the generated combustible gases (Lackner, 2010, p.123).
Underfeed stokers can be easier controlled than grate furnaces because of their simple load control with the screw conveyor and a good partial-load burning behavior. In contrast, ash accumulation on the fuel bed and ash removal can cause problems and difficulties. Sintered or melted ash particles on the fuel layer surface may lead to unstable combustion conditions. Therefore, underfeed stokers are more suitable for fuels with low ash content and small particle sized up to 50 mm. Ash-rich fuels can require the implementation of efficient ash removal systems (Lackner, 2010, p.123).

Fluidized-bed combustion

Fluidized-bed combustion reactors are very similar to fluidized-bed gasifiers. They consist of a vessel and a gas distribution plate at the bottom. The fluidizing medium, usually air for the combustion process, flows from below the distribution bed upwards into the fluidized bed. The fluidized bed consists of granular solids which are kept in a fluidized state by the

air flowing through the bed. The two most applied reactor designs are bubbling fluidized-bed (BFB) and circulating fluidized-bed (CFB) systems.

Bubbling fluidized-bed reactors have superficial gas velocities of 1-2 m/s and contain bed materials with an average diameter of 700-1000 µm. Fuel feedstocks of up to 100 mm are possible, but the average feedstock size is about 50 mm. The gas flow transports most of the generated ash as fly ash out of the fluidized-bed reactor and has to be separated from the gas stream in adequate dedusting equipment (Kaltschmitt et al., 2009, p.516).

Temperature control of the fluidized bed is typically realized either by submerged heat exchanger plates into the fluidized bed or by regulating the combustion air in the reactor to generate understoichometric combustion conditions in the bed. Reactors with submerged heat exchangers use most of the combustion air as the fluidizing medium (primary air) and only a fraction of the combustion air is introduced as secondary air. Implementation of submerged heat exchanger plates is usually avoided as they are subject to erosion by the bed material and feedstock particles. Furthermore, operation at half capacity reduces the bed temperature and the combustion temperature. Temperature control with understoichometric combustion conditions in the fluidized bed is the prefered way in recent years. To keep the temperatures within the required limits, a flue gas recirculation is required for the reactors. Parts of the fuel is gasified in the fluidized bed and the postcombustion of the generated gases takes place with the secondary air in the freeboard above the bed. The temperature in the bed is controlled with the amount of oxygen in the fluidizing air.

Circulating fluidized-bed reactors operate at higher superficial velocities than BFB reactors. This leads to bed material discharge out of the reactor, called entrainment. The bed material has to be separated from the gas stream with cyclones and recirculated into the fluidized-bed reactor. Temperature control can be achieved by cooling part of the bed material prior to recirculation into the reactor (Kaltschmitt et al., 2009, p.519).

Entrained-flow combustion

Entrained-flow combustion is also called dust firing and requires smaller particles as fuel feedstock. Therefore, only small biomass can be implemented like wood chips, sawdust and other fine-grained residues. The fuel feedstock is mixed with the combustion air and pneumatically transported with the air into the combustion chamber. Secondary air is often introduced in the combustion chamber and can also be added at different stages in the chamber. The water content of the fuel is very crucial and must be under 15-20 % to ensure auto-ignition of the fuel in the combustion chamber (Kaltschmitt et al., 2009, p.520).

The different reactor designs described above are suitable for thermochemical conversion of biomass. This thesis focuses on fluidized-bed systems and the interaction of biomass ash and bed material in the reactors.

2.2 Bed materials in fluidized-bed systems

This section describes different bed materials implemented in fluidized-bed systems. A variety of bed materials will be described in terms of general composition, degree of implementation in fluidized-bed systems and the research progress up to the point of writing of this thesis. In general, it can be noted that a couple of bed materials are broadly used in research and commercial applications, whereas others can be described as more exotic in terms of implementation. The commercially less used bed materials are often used as benchmark materials in small-scale laboratory reactors or appointed to evaluate the influence on combustion and gasification conditions and products. A short introduction on the function of bed materials follows.

Bed materials in fluidized-bed gasification and combustion systems are typically coarse, granular solids. A fluidizing medium is required for fluidization of the solid material. The fluidizing medium, typically a gas, is introduced from below a distribution plate where the bed material rests on. If the velocity of the fluidizing medium passing through the bed material exceeds the minimum fluidization velocity for the specific bed material, the solid particles become suspended by the gas flow and act as a pseudo-fluid in the reactor vessel, called a fluidized bed.

The fluidized bed in the reactor has various advantages and functions for the gasification and combustion processes. The amount of bed material together has a large heat capacity that serves as a heat reservoir in the reactor. Gasification and combustion can be maintained without additional heating of the reactor. The fluidization of the bed material creates turbulence in the bed and ensures good mixing of the bed material and the fuel. Due to the effective mixing conditions the heat in the reactor can be stored evenly in the bed material resulting in a relatively homogeneous temperature distribution within the bed material (Lackner, 2010, p.471). It also serves as heat carrier in a dual-fluidized gasification reactor (see section 2.1.1). The mechanical property of a bed material also needs to be considered as rupture and abrasion cause bed material loss over time. Some bed materials are inert solids with no or negligible effects on reactions in the reactor, whereas others can be catalytic ac-

tive towards tar conversion and reduction in biomass gasification applications. The catalytic active bed materials facilitate the tar reduction reactions and reduce the overall production of tar in gasification processes which in turn reduces operational problems caused by tar condensation in low-temperature plant equipment.

Quartz sand, typically silica SiO_2, is a bed material that has been frequently tested in a number of applications in conjunction with fluidized-bed systems.
Agglomeration tests with quartz sand and biomass ash from corn straw, rice straw and wheat straw in various fluidization gas mixtures of H_2, CO_2, N_2, steam or air were performed. The defluidization temperature in CO_2 and air is almost the same, whereas for H_2 and steam it is significantly lower. In a reducing atmosphere with steam, agglomeration for corn straw and rice straw appeared to be coating-induced, while for wheat straw melt-induced. In H_2 and air atmospheres, agglomeration presented itself as melting-induced (Ma et al., 2016). Various experiments by other authors with different fuels have been performed regarding agglomeration characteristics with quartz sand. For example, co-firing of municipal sewage sludge and wheat straw in a 5 kW BFB reactor showed improved performance of those problematic fuels as opposed to separate combustion. Particularly, bed defluidization tendencies were greatly reduced due to a shift in agglomeration characteristics and deposit build-up rates were improved (Skoglund et al., 2013).

Experiments on the time-dependence of bed particle layer formation in fluidized quartz bed combustion of wood-derived fuels were implemented on quartz bed material samples from three different sources: a bench-scale 5 kW BFB reactor, a full-scale 30 MW_{th} BFB plant, and a full-scale 122 MW_{th} CFB plant. The campaign durations were 40 hours, 23 days and 6 days, respectively. Significant differences in layer morphology and composition were found within particles of different ages (He et al., 2014). The gathered information was further analyzed in conjunction with phase diagrams, chemical equilibrium calculations and a diffusion model to propose a mechanism for quartz bed particle layer formation in fluidized-bed combustion of wood-derived fuels. The introduced mechanism comprises 3 stages of layer formation: reaction of potassium with quartz forming low-melting K-silicates, diffusion of calcium in the melt, and formation of solid Ca-silicate layers (He et al., 2016).

Fresh and used quartz bed samples from a bubbling fluidized-bed combustion plant in Austria were investigated for their catalytic activity in gasification reactions. The used bed material was sampled during normal operation in the 48 MW plant with wood chips as fuel feedstock. The operating temperature of the BFB combustor was 740℃. The samples were investigated in a lab-scale test rig at Vienna University of Technology. Fresh quartz material showed no signs of catalytic activity. The used bed material is subject to bed particle coatings and particle layer formation due to interactions with the biomass ash. Results showed that the formation of calcium (Ca)-rich layers on bed particles yields a catalytic active surface regarding the water-gas-shift reaction and steam reforming of tars from biomass gasification (Kuba et al., 2016a).

Quartz sand is likely to be introduced into a fluidized-bed system with the fuel feedstock as impurity. This was the case in a combined heat and power plant (CHP) in Senden, Germany. With a fuel capacity of 15 MW, the full-scale power plant houses a dual fluidized-bed steam gasifier operated with olivine as the primary bed material. The quartz sand was acknowledged as impurity since it remains in the fluidized bed and acts as bed material as well. This circumstance was used advantageously to test the material for basic suitability in dual fluidized-bed gasification systems in terms of agglomeration behavior and particle fracturing at certain temperatures. Data was acquired over a period of 3 weeks during continuous operation. Results showed that quartz is a possible candidate as alternative bed material, but would bring challenges regarding agglomeration and deposit build-up (Kuba et al., 2016c).

A recent study focused on the bed material depositions on walls, cyclones and return legs in fluidized-bed combustion systems. These depositions partly originate from sticky fragments of alkali-rich silicates formed after crack formation in older quartz bed particles. Bed samples have been taken from two full-scale fluidized-bed systems: a 30 MW_{th} BFB, and a 90 MW_{th} CFB. Both feedstocks comprised woody-type biomass. Bed samples were taken over a period of 23 and 13 days, respectively. The bed material exchange rate was the same as during normal operation. A 3-phase crack layer formation process for quartz sand was proposed based on the results. Phase 1 involves the formation of a thin inner layer

surrounding the quartz bed particle, typically enriched in calcium. Phase 2 comprises crack formation through the inner layer down to the interface between inner layer and quartz particle core. These cracks allow the diffusion of gaseous alkali to react with the silicates in the quartz particle core, forming crack layers. The reaction is accelerated in Phase 3 and accompanied by formation of bridges between the crack layers probably leading to particle breakdown into smaller alkali-silicat-rich fragments. Furthermore, a weekly replacement of the complete bed material was recommended to avoid bed material deposition issues and increase the operation time (He et al., 2017).

Olivine, with the general formula $(Mg,Fe)_2SiO_4$ a magnesium iron silicate, is a bed material widely used in full-scale fluidized-bed systems for its mechanical properties and catalytic activity in gasification processes.

The effects of non-quartz bed material on agglomeration characteristics compared to quartz have been investigated during fluidized-bed combustion of biomass with controlled agglomeration tests described by Öhman & Nordin (1998). Bark representing woody biomass with typically high calcium content (CaO 38.7 % mass fraction in ash), potassium-rich olive residue (K_2O 33.0 % mass fraction in ash) and wheat straw representing agricultural residues with high potassium and silica content (K_2O 12.5 %, CaO 10.4 % mass fraction in ash) were used as fuels in the experiments. Results showed different reactions between the bed material and the fuel depending on the fuel ash composition leading to different agglomeration behavior in the reactor. Olivine increased the combustion time of olive residue prior to agglomeration, but had no significant influence during bark combustion. The agglomeration behavior of wheat straw during combustion was not influenced by olivine (De Geyter et al., 2007).

Further experiments on agglomeration characteristics in a 5 kW bench-scale BFB combustor used willow, logging residues, wheat straw, and wheat distiller's dried grain with solubles (DDGS) as fuel feedstock. For 8 hours, a pre-determined amount of fuel was burned at a constant temperature of 800 °C, for wheat straw 730 °C. Hereafter, the fuel feed was stopped and the temperature increased until defluidization occured. Chemical equilibrium calculations were performed to interpret the experimental findings. Both woody fuels yielded

relatively homogeneous inner reaction layers mainly dominated by Mg, Si, and Ca. The outer coating layers with more granular structure resembled the fuel ash composition. Layer formation and agglomeration with wheat straw and DDGS fuel was connected to bed particles sticking together by partly molten ash derived K-silicates for wheat straw and K-Mg-phosphates for DDGS (Grimm et al., 2012a).

The effects of bed material coatings on tar reduction were examined with fresh and used olivine in a 100 kW dual fluidized-bed gasifier. The used olivine samples were taken from the DFB biomass-steam gasification plant in Güssing, Austria, with 8 MW fuel capacity. Wood pellets were used as fuel in the pilot-plant experiments. Results showed that used olivine increased the hydrogen and carbon dioxide content in the product gas, while carbon monoxide was reduced. It promoted the exothermic water-gas-shift reaction leading to lower energy demand for the gasification. The tar content was reduced by approximately 80 %. The effects were attributed to the formation of Ca-rich layers on the used olivine (Kirnbauer et al., 2012). The Ca-rich layers comprise two layers, an inner and an outer layer. The inner layer consists mainly of calcium silicates with a more homogeneous appearance, while the composition of the outer layer is similar to the fine ash presenting a more heterogeneous appearance. Woody biomass was used as fuel feedstock with calcium (Ca) as the dominating element in the biomass ash and additional Ca-rich additives were introduced to improve the catalytic properties of the bed material in terms of tar reduction (Kirnbauer & Hofbauer, 2011). A comparison of the elemental composition between the particle surface and the outer layer showed similar compositions with Ca in the highest concentration (approximately 50 wt-%), followed by magnesium (approximately 20 wt-%) and silicon (approximately 15 wt-%). The effect of different atmospheres in the reactor on the particle surface composition was investigated as well. The experiments showed no significant impact on the particle surface composition for both, the reducing atmosphere in gasification and the oxidizing atmosphere during combustion Kirnbauer & Hofbauer (2013).

A study on the catalytic effect of olivine and Fe-impregnated olivine regarding the reforming of tar and methane was performed in a 150 kW DFB allothermal gasifier at Mid Sweden University (MIUN). Comparisons were drawn with the reactor operation in single BFB mode.

Results showed differing catalytic behavior between DFB and BFB operation. The BFB operation mode yielded higher tar and methane content with higher hydrogen and carbon monoxide concentrations compared to the DFB setup. No clear advantage of Fe/olivine over olivine concerning catalytic reforming of tar and methane could be shown (Göransson et al., 2015). The catalytic activity of olivine in DFB gasification was also shown in experiments for bed material comparison by Berdugo Vilches et al. (2016).

Experiments on the enhancement of the catalytic activity due to olivine particle coatings regarding the water-gas-shift (WGS) reaction and steam reforming of toluene were performed in a lab-scale test rig at three different temperatures (750 ℃, 800 ℃, 850 ℃). Used olivine showed notably higher catalytic activity towards the WGS-reaction compared to fresh olivine. The steam reforming experiment of the model tar compound toluene resulted in higher conversion efficiencies for used olivine compared to fresh olivine. The experiments showed increasing catalytic activity (WGS) and increasing conversion efficiencies with increasing temperatures (Kuba et al., 2016a). An updated and more detailed mechanism of layer formation on olivine bed particles was proposed after experiments in an industrial DFB gasification plant with wood as feedstock. The suggested mechanism involves a solid-solid substitution reaction, where calcium is incorporated into the crystal structure of olivine by replacing either iron or magnesium atoms (Kuba et al., 2016b). Lab-scale experiments were carried out to investigate the influence of Ca-rich olivine coatings on the conversion of intermediate products (1H-indene and methane) from the decomposition of biomass tars during gasification. Results showed that used olivine with Ca-rich layers had significantly higher catalytic activity towards 1H-indene conversion compared to fresh olivine. Used olivine converted approximately 70 %, whereas fresh olivine approximately 24 %. Carbon monoxide (CO) is next to hydrogen (H_2) a product of the 1H-indene conversion. The subsequent water-gas shift reaction further converts CO to carbon dioxide and hydrogen. The Ca-rich layers on used olivine showed significant influence on the water-gas shift reaction as well. Conversely, used and fresh olivine exhibit insufficient catalytic activity towards methane conversion (Kuba et al., 2016d).

Olivine needs to undergo an activation process before it becomes catalytic active for gasi-

fication reactions, called calcination. The change in activity is commonly attributed to Fe migration in the particle occuring during calcination (Christodoulou et al., 2014). Experiments with non-calcined olivine were carried out to gain insights in the activation process and the consequences for the performance of the gasifier regarding gas composition, tar load and efficiency. The aging/activation of olivine was observable by changes of the product gas composition as already described above (Marinkovic et al., 2015b).

Another study developed and tested a thermodynamic equilibrium model to assess the risk of bed agglomeration in gasification and combustion reactors of a DFB gasifier using forest residues as biomass feedstock. The study aimed to predict composition and melting behavior of the biomass ash and the bed particle layers by means of thermodynamic equilibrium calculations and chemical fractionation technique. Results showed a good agreement between the modelling results and the experimental observations (Moradian et al., 2016).

Calcium oxide (CaO) is sometimes used as a reference material in fluidized-bed gasification experiments because of the high Ca content. The catalytic effect of CaO on the conversion and reduction of tar compounds (Delgado et al., 1997) in biomass gasification applications is compared to the catalytic effect of other bed materials under similar conditions. Implementation of CaO as bed material in fluidized-bed systems can increase the used amout of bed material during continuous operation. The hardness of CaO (Mohs' scale 3-4) is lower compared to other bed materials like quartz (Mohs' scale 7), olivine (Mohs' scale 6.5-7), and feldspar (Mohs' scale 6-6.5). The decreased hardness of CaO results in lower abrasion resistance of the CaO particles. Lower particle abrasion resistance is detrimental in the dynamic mixing conditions of a fluidized bed and causes increased abrasion and breakage of particles. As a result, the size of particles is continuously reduced over time which leads to particle entrainment and loss of bed material.

Bauxite was used in mixtures with silica sand of different ratios as bed materials to evaluate the performance of the mixtures with regard to alkali compound interaction, bed agglomeration tendency and overall reactor performance. Bauxite (88.5 % aluminum calculated as Al_2O_3) and mixtures of bauxite and silica sand were used as bed materials in a 12 MW fluidized-bed boiler with wood pellets as fuel. The simplified laboratory experiments used

K_2CO_3 and $CaCO_3$ as biomass ash components of major importance. The set laboratory conditions were 800 °C for a period of 9 hours. The conclusions suggest that with increased amounts of bauxite in the bed material mixtures with silica sand, bed agglomeration decreased but did not stop. Calcium did not cause agglomeration with the tested bed materials but formed a Ca-rich layer around the particles. The laboratory experiments seemed to reflect the observed processes in the industrial scale boiler (Knutsson et al., 2014).

Bauxite was further used to investigate the influence of interactions between biomass ash and bauxite bed material on the performance of an indirect gasification system in a DFB setup. In Chalmers DFB system, where the boiler is a circulating fluidized-bed and the gasifier is a bubbling fluidized-bed, the experiment was carried out over 9 consecutive days. The gasifier was only in operation during daytime, whereas the boiler was running continuously. Wood chips where used as fuel in the CFB boiler and wood pellets in the gasifier. Two main conclusions were drawn from the experiment. Firstly, bauxite experienced a change in catalytic properties which enhanced the fuel conversion. Overall carbon conversion to permanent gases increased due to a 40 % decrease in tar yield and an enhanced char conversion (36 %). Secondly, the aging of bauxite in the system promoted a significant increase in its oxygen transport capability, limiting its implementation as bed material in a DFB system with gasification purposes (Marinkovic et al., 2016).

In the same DFB system, the effects of bauxite on product gas and tar yield were compared to olivine and quartz sand. Results showed that bauxite is a suitable in-bed catalyst for the water-gas shift (WGS) reaction and capable of doubling the H_2/CO ratio compared to quartz sand. Conversely, bauxite exerted little influence regarding the CH_4 yield. The tar removal effect of bauxite was evaluated via observation of SPA-measureable tar (excluding BTX). Lower tar contents were registered, but the effect was weaker compared to olivine. The oxygen transport capabilities of bauxite, as described by the aforementioned experiments, were confirmed and partly attributed to the ash load of the material. The oxygen transport capability results in a higher CO_2 yield compared to olivine, which usually leads to lower H_2 production. The reduced hydrogen production due to the higher oxygen transport capability of bauxite was offset by increased catalytic effects towards the WGS-reaction, tar reforming,

and char gasification (Berdugo Vilches et al., 2016).

Ilmenite is black iron-titanium oxide and the primary ore of titanium. The ideal chemical composition is $FeTiO_3$ with different solid solution series in place, substituting the iron with magnesium and manganese forming $MgTiO_3$ and $MnTiO_3$. At high temperatures, a third solution series exists with hematite (Fe_2O_3).

Researchers at Chalmers University of Technology used ilmenite as the catalytic material in a dual fluidzed-bed gasifier to reduce the production of tar during gasification. Mixed with silica sand, ilmenite was part of the bed material to investigate the impacts on the process. Higher fluidization of the bed material resulted in a higher impact of ilmenite on the water-gas shift reaction but had the opposite effect for tar reduction, with higher conversion at low fluidization levels. The addition of 12 % ilmenite as bed material reduced the tar yield by approximately 50 %, but increased the fraction of heavy tars. A 10 % reduction in cold gas efficiency was compensated by additional char combustion, conversion of organic compounds and shifting the gas composition towards equilibrium (Larsson et al., 2014).

A study at Chalmers University of Technology evaluated the physical and chemical changes of ilmenite during the combustion of biomass in the Chalmers 12 MW_{th} circulating fluidized-bed (CFB) boiler. The CFB usually uses 2000 kg of silica sand as bed material. In the four-day experiment, up to 40 wt-% (800 kg) of the silica sand was replaced by ilmenite to evaluate how the ash components of woodchips interact with the bed material. Findings show the ash component potassium diffusing homogeneously into the ilmenite particles forming the potassium titanium oxide KTi_8O_{16}. Segregation was observed in ilmenite as the iron migrates to the surface and the titanium becomes enriched in the particle core. Furthermore, calcium-enriched layers were found on each side of the iron layer (Corcoran et al., 2014).

Ilmenite was also used as a reference bed material for the oxygen transport effect in DFB gasification (Berdugo Vilches et al., 2016). The results provided the groundwork for further experiments. The long-time experiments in the DFB system at Chalmers University of Technology with the boiler/gasifier loop (input 12 MW_{th} and 2-4 MW_{th}, respectively) used ilmenite

as the oxygen-carrying bed material in two experiment campaigns. In more than 800 hours of accumulated operational time, ilmenite was used as bed material to investigate the influence of fluidization velocity, fuel feeding rate and bed material circulation rate on biomass conversion. The operating temperature in the fluidized-bed gasifier was around 830 °C. The fuel fed to the gasifier was commercial wood pellets from spruce trees. In respect of the bed materials durability, the authors noted that ilmenite is able to undergo redox cycles for long operating times (Berdugo Vilches et al., 2017).

Feldspar represents a group of minerals with the chemical composition $X(Al,Si)_4O_8$. The general X in the formula stands for one of the seven ions K^{1+}, Na^{1+}, Ca^{2+}, Ba^{2+}, Rb^{1+}, Sr^{2+}, and Fe^{2+}. The common forms of felspar include potassium, sodium and/or calcium, and can be classified chemically as members of the ternary system $NaAlSi_3O_8$-$KAlSi_3O_8$-$CaAl_2Si_2O_8$, as shown in Figure 2.7. Those feldspars can be subdivided into two main groups: alkali-feldspars and plagioclase-feldspars. In alkaline feldspars, potassium (K) is rather bound to the tetrahedra structure as opposed to sodium (Na) and calcium (Ca) in the case of plagioclase feldspars (Greenwood & Earnshaw, 1995).

An earlier study acknowledged the presence of non-quartz minerals in fluidized-bed combustion systems when using natural sand as bed material. Potassium feldspar (K-feldspar) and plagioclase feldspar (Na,Ca-feldspar), the later specifically labradorite, were first investigated regarding agglomeration behavior in fluidized-bed combustion of biomass fuels. Three different fuels were used as feedstock: Ca-rich bark, K-rich olive residues, and Si- and K-rich wheat straw. Results showed that both composition and interaction of bed material and biomass ash are the main factors influencing bed agglomeration behavior (De Geyter et al., 2007).

The catalytic activity of (supposedly) fresh alkaline feldspar, $(K,Na)AlSi_3O_8$, was investigated for upgrading a biomass-derived producer gas from a gasifier. The producer gas was a slip-stream from the Chalmers 2-4 MW indirect biomass gasifier and used as the fluidizing medium for the experiments in a single BFB reactor. The material was tested at 700 °C, 800 °C, and 900 °C, over a total experiment time of 3 hours. Results showed that feldspar functions as a tar reforming catalyst and exhibits suitable mechanical properties for fluidized-

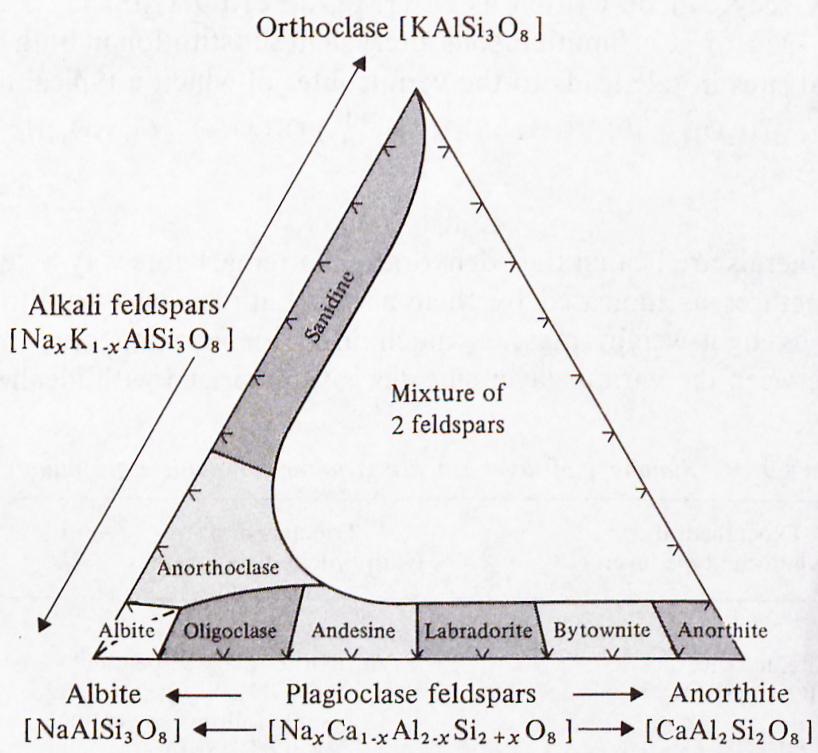

Figure 2.7: Ternary phase diagram for feldspars (Greenwood & Earnshaw, 1995, p.414)

bed operation. A low oxygen transport capability was attributed to the tested feldspar and no agglomeration behavior was detected. It should be noted, that the conditions for the experiment comprise a downstream operation after a gasifier unit at which point the biomass ash would already be removed (Berguerand et al., 2016).

Evaluation of feldspar particles sampled from a DFB gasifier with 15 MW fuel capacity showed promising results for feldspar as an alternative bed material in fluidized-bed systems. Feldspar particles were not intentionally used as bed material in the power plant which operates with olivine as regular bed material. Feldspar and quartz particles were introduced as impurites with the fuel feedstock, the logging residues. Since the feldspar and quartz particles remain in the reactor and act as bed material, the authors used it to their advantage to compare for agglomeration behavior and fracturing at typical process temperatures. Results showed that the layers on K-feldspar, similar to olivine, displayed significantly lower agglomeration tendency compared to quartz particles from the same reactor. Moreover, the layers formed on K-feldspar were characterized with higher stability in comparison

to olivine and quartz particle layers, where significant fracturing was detected (Kuba et al., 2016c).

Blast-furnace slag, a by-product from the production of iron in a blast furnace, was used as alternative bed material for the combustion of biomass in the 12 MW Chalmers CFB system. The major constituents of blast-furnace slag are calcium-magnesium-aluminum silicates. The experiments aimed to study different means of mitigation for alkali-related problems. Specifically, to assess the influence on bed agglomeration tendency and deposit formation. The experiment was set up as a long-time experiment of up to 60 hours of continuous operation. Wood chips and wood pellets together with straw pellets were introduced as fuels. The bed temperature at bottom and top were 870 °C and 851 °C, respectively. For the first 12 hours of operation, the agglomeration temperature for the bottom bed samples were above the maximal experimental temperature (1100 °C). After about 27 hours the agglomeration temperature was approximately 1000 °C, and after about 47 hours it was approximately 970 °C. Particle cross-sections from the bottom bed samples showed that most particles have no layer formed at all, but on some particles, layers containing potassium, calcium and silicate have formed. The alkali accumulated in the bed material does not react with the bed particle surface, which is in accordance with observations in the bench-scale experiments by Brus et al. (2004). Therefore, the use of blast-furnace slag as alternative bed material counteracts bed agglomeration (Davidsson et al., 2008).

Mullite, an alumina sand, was used as bed material in a bubbling fluidized-bed gasifier at Texas A&M University. The goal was to study the gasification characteristics of wheat straw with air as the gasification agent. 40 kg of fresh mullite was used as bed material and the gasification temperature was 760 °C. Observations concerning defluidization showed that temperature alignments within the fluidized bed point to the onset of defluidization at approximately 750 °C. To avoid bed agglomeration above 800 °C, the use of alternative bed material alone is insufficient and reactor design must bed considered as well (Mac an Bhaird et al., 2014).

Manganese ore as active bed material was used in a mixture (50/50 wt-%) with silica sand for the combustion of methane with variable air-to-fuel ratios in a lab-scale circulat-

ing fluidized-bed combustor. The aim was to study the effect of manganese ore as an active oxygen carrier for the use in Oxygen Carrier Aided Combustion (OCAC) processes. The exhaust concentration of carbon monoxide was chosen as the main performance indicator for this experiment. Manganese ores from two different suppliers were used and both underwent pre-treatment at 950℃ for 24 hours prior to application. It was shown that the mixture of manganese ore and silica sand as bed material significantly reduced the exhaust concentration of carbon monoxide compared to silica sand as bed material alone (Källen et al., 2015).

Pre-calcined manganese ore provided by Sibelco (Belgium) was used in Chalmers 12 MW semi-commercial CFB boiler/gasifier system to study manganese ore as bed material for OCAC application. The calcination conditions were not provided by the supplier but were estimated at 600-800℃ for more than one hour in a rotary kiln. Various mixtures with silica sand and manganese ore as bed material were implemented for the combustion of mostly pine and spruce wood chips. The experiments concluded for manganese ore to be a viable option to improve the performance of existing CFB boilers. No problems were encounterd for attrition and agglomeration with manganese ore. A 10 % substitution of silica sand with manganese ore allowed to reduce the air-to-fuel ratio significantly without generating large amounts of carbon monoxide. However, the use of 100% manganese ore resulted in larger amounts of carbon monoxide than for the silica sand (Rydén et al., 2016).

Long-time experiments in the DFB system at Chalmers University of Technology with the boiler/gasifier loop (input 12 MW_{th} and 2-4 MW_{th}, respectively) use manganese ore as the oxygen-carrying bed material in one experiment campaign. Prior to operation, the manganese ore was pre-treated at about 800℃ resulting in some sintering and manganese beeing present as Mn-(III)-oxide. In about 500 hours of accumulated operational time, manganese ore was used as bed material to investigate the influence on biomass conversion of fluidization velocity and fuel feeding rate. Operating temperature in the fluidized-bed gasifier was around 830℃. The fuel fed to the gasifier were commercial wood pellets from spruce trees. Results showed that manganese ore is suitable as an oxygen carrier material for large-scale chemical looping combustion (CLC) (Berdugo Vilches et al., 2017).

Manganese ore was also tested for upgrading biomass derived product gas in a chemical-looping reforming (CLR) reactor. The reformer section was set up as a circulating fluidized bed to improve the gas-solid contact time. The catalytic activity was monitored at 800℃, 850℃, and 880℃ using raw gas from the Chalmers 2-4 MW biomass gasifier. The tests were carried out over a total of 4.5 hours. Manganese ore showed promising catalytic properties towards tar components and upgrading the gas composition. The authors suggested to consider the ore as a primary measure in the first stage of gasification. SEM/EDX analyses showed signs of agglomeration of the material due to contamination with silica sand particles in the preparation phase (Marinkovic et al., 2015a).

Magnesite was used as alternative bed material for experiments in a pilot scale air-blown bubbling fluidized-bed (BFB) gasifier at the University of Limerick, Ireland. The used feedstock was cardoon (Cynara cardunculus L.), an energy crop also called artichoke thistle. Two experiments with magnesite were executed with gasification temperatures of 700℃ and 800℃. Results showed that magnesite provided better gasification performance at the lower temperature of 700℃. It had positive effects on product gas composition, biomass conversion, LHV, gas yield and char conversion. However, tar concentration remainded high in the product gas and would require downstream gas cleaning. Magnesite showed higher catalytic activity at 800℃ (Serrano et al., 2016).

Sepiolite, with the empirical formula $Mg_8Si_{12}O_{30}(OH)_4(OH_2)_{48}H_2$, is a high porosity clay mineral and was used as alternative bed material in a lab-scale bubbling fluidized-bed (BFB) gasifier. The feedstock was cardoon (Cynara cardunculus L.), an energy crop also called artichoke thistle. The amount of bed material for the sepiolite experiment was about 100 grams and the reactor temperature was 850℃. Results showed that sepiolite increased the elapsed time until defluidization, compared to silica sand. Bed agglomeration with sepiolite occured as a whole, as opposed to only partial bed agglomeration observed with other bed materials. Defluidization for each experiment with different fluidization velocities occured within 3000 seconds, that is, within 50 minutes of operation (Serrano et al., 2015).

The effect of sepiolite on gas composition and tar production was also investigated in the lab-scale bubbling fluidized-bed gasifier. Comparisons were drawn with silica sand as bed

material. The results showed no improvement in product gas composition. More CO_2 and less CO were produced, and hydrogen production showed no clear trend. Carbon conversion and LHV were also reduced. On the other hand, sepiolite reduced tar generation up to 50 %, specifically tertiary PAH tars (Serrano et al., 2017).

The bed materials described in this chapter display various chemical compositions and properties. These compositions and properties need to be tested under combustion and gasification conditions in fluidized-bed systems to evaluate their applicability regarding these thermochemical conversion processes. The research results described for the bed materials highlight that the behavior of bed materials changes significantly with different combinations of bed material, fuel feedstock, and process conditions. However, the amount of research conducted to investigate different bed materials varies significantly between different materials. Some bed materials were subject to short-term lab-scale experiments, while others were tested in long-term industrial-scale experiments as well. Lab-scale experiments can generate very valuable insights into the behavior of bed materials during the initial hours of operation which can help identify layer formation mechanisms or agglomeration problems. However, to evaluate the suitability of bed materials for long-term use in industrial-scale applications, elaborate experiments over longer periods should be conducted to put the results obtained from short-term experiments to the test. A thorough evaluation regarding the suitability of a bed material for a certain conversion process can only be achieved with a wide range of different experiments.

Another important aspect to consider when researching different bed materials is their availability. Bed materials only available in certain regions will probably limit their implementation to those regions. The research conducted on these bed materials and the knowledge gained from the experiments will be difficult to adapt to other bed materials. Bed materials should be readily available and inexpensive. Research conducted on bed materials universally available and easy to acquire will ensure easier transfer of knowledge which increases their potential to be implemented in various regions without limitations due to restricted availability.

2.3 Biomass fuels

The term ‘biomass‘ defines all materials with organic origin, that is, carbonaceous matter (Kaltschmitt et al., 2009, p.2). This is one of many versatile definitions for biomass to find. Biomass resources display a wide variety of constituents which makes it challenging to find a precise definition for biomass covering all possibilites in a short phrasing. In terms of biomass classification, peat is often regarded as the boundary separating fossil fuels from biomass. Differencies in opinions exist on whether peat accounts for biomass or fossil fuel (Kaltschmitt et al., 2009). Three main types of biomass resources can be distinguished: living forests, energy crops, and together residues, by-products, and wastes (Nikolaisen & Jensen, 2013).

From these biomass resources a variety of biomass fuels can be classified into different types: forest wood, herbaceous biomass, forest and agricultural waste, industrial and household waste, and modified biomass fuels (Lackner, 2010).
Forest wood comprises wood blocks and wood chips. Wood blocks are certainly too bulky as a biomass fuel in fluidized-bed combustion and gasification, whereas wood chips can be successfully incorparated as fuel feedstock. Examples for the implemented forest wood are: willow, poplar, pine, and spruce from temperate climate zones, and gum tree as well as eucalyptus from tropical and sub-tropical climate zones (Rosendahl, 2013).
Herbaceous biomass is from plants with a non-woody stem and which grow back or die at the end of the growing season. Examples are: miscanthus, triticale, switchgrass, rapeseed, sorghum.
Forest and agricultural waste are by-products from forestry, wood-working and agricultural operations. Forest waste includes remains from timber production and wood-working, e.g. logging residues like roots, stumps, stems, and branches as well as bark and saw dust. Agricultural waste contains for example manure and harvest waste. Manure is produced by farm animals like poultry, cattle and pigs, and harvest waste from various crops generates corn stalks and wheat straw for example.
Miscellaneous industrial and household waste constitute waster paper, municipal solid waste

(MSW), waste from food industries and sludge.
Modified biomass fuel comprises torrefied wood, wood pellets and char coal.
A clear separation of those categories is not always possible as it is the case for grain screenings and waste from shea, sunflower, olive, or rape products. They originate from an agricultural background, but often accrue during industrial post-processing and production. Therefore, they can also be viewed as industrial biomass waste.

General categorization is helpful for describing the origin of the biomass resources, but for a successful implementation in fluidized-bed combustion and gasification the physical and chemical characteristics of the solid biomass fuels are of higher importance.

2.3.1 Characteristics and properties of solid biomass fuels

Classifying various fuels and assigning them to groups is an important means to deduce and estimate characteristics and properties for comparable fuel feedstock. Fuels assigned to a particular group tend to exhibit similar behavior during thermal conversion processes. From the classification of a fuel, especially a new one for a certain process, an estimate can be drawn about the potential implementation in that process. One way of classifying fuels is according to their atomic ratio (Basu, 2010).

The atomic ratio of a fuel is dependent on the hydrogen (H), oxygen (O), and carbon (C) content of a certain fuel. Those elements are the main constituents of biomass fuel. It is common to represent fuels in the so-called van Krevelen diagram. Two atomic ratios based on the composition of a dry and ash-free fuel, H/C and O/C, are usually plotted on the x- and y-axis of that diagram. One understanding, gained from the classification according to atomic ratios, is the correlation of heating values and ratios, as shown in Figure 2.8.

Biomass contains a number of different organic compounds, inorganic constituents and moisture which translate to different properties of different fuels. The composition and properties of a biomass certainly influence a conversion process and need to be known before implementation. Whether for the thermal design of a new biomass conversion plant or the new implementation of a certain biomass in an existing system, it is necessary to know the

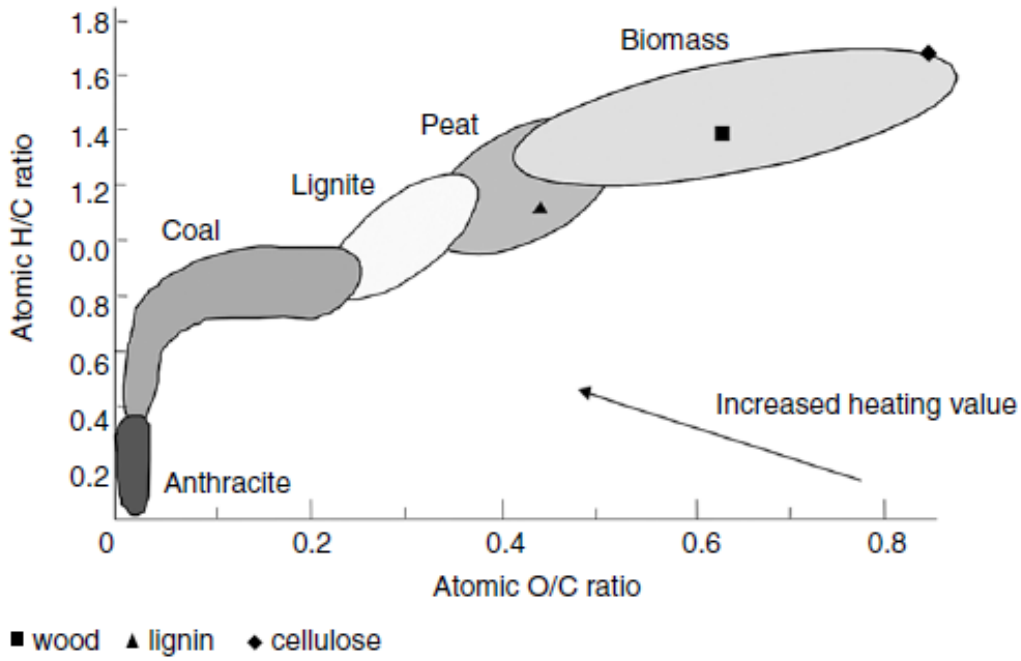

Figure 2.8: Classification of solid fuels according to their O/C and H/C ratios (van Krevelen diagram) (Basu, 2010, p.39)

composition of a fuel and its energy content for sufficient operation. Three important properties describe the composition and energy content of fuel: ultimate analysis, proximate analysis, and heating values.

Ultimate analysis gives the composition of solid fuels based on the principal elements carbon (C), hydrogen (H), oxygen (O), nitrogen (N), sulfur (S), chlorine (Cl), inorganic constituents (ash), and moisture.

Proximate analysis expresses the composition of the fuel regarding total components such as volatile matter (VM), ash, moisture, and fixed carbon (FC). Volatile matter is the condensable and non-condensable vapor released during heating of the fuel. Ash is the solid residue that remains after the fuel is completely burned. The amount of fixed carbon differs from the carbon content measurend in the ultimate analysis. Fixed carbon in the proximate analysis only includes the carbon that represents char after devolatilization, and excludes the carbon of volatile matter.

Heating values represent the amount of thermal energy released by the fuel in the conver-

sion process. Two separate values are of relevance: higher heating value (HHV) and lower heating value (LHV). HHV is defined as the amount of heat released by unit of mass or volume by the fuel when the fuel is combusted. It is the amount of heat released from initially 25℃ to the point where the products have returned to a temperature of 25℃ after conversion. This includes the latent heat of water vaporization. Conversely, the LHV excludes the latent heat of water vaporization and is defined as the heat released by fully combusting a certain quantity reduced of the latent heat of water vaporization. In general, an experimental method to determine heating values for fuels is the most reliable one, but various equations and correlations exist to estimate the heating value of fuels (Basu, 2010).

Examples for different biomass fuels and their characteristics are shown in Table 2.1.

Table 2.1: Proximate and ultimate analysis of different biomass fuels (Vassilev et al., 2010),(ECN, 2017)

Biomass fuels	**Proximate analysis (db)**			**Ultimate analysis (daf)**					**LHV[c] (daf)**
	FC[a] [%]*	VM[b] [%]*	Ash [%]*	C [%]*	H [%]*	O [%]*	N [%]*	S [%]*	[MJ/kg]
Wood and woody biomass									
Birch bark	19.4	78.5	2.1	57	6.7	35.7	0.5	0.1	23.2
Pine bark	24.4	73.7	1.9	53.8	5.9	39.9	0.3	0.07	20.2
Poplar	12.3	85.6	2.1	51.6	6.1	41.7	0.6	0.02	18.8
Poplar bark	17.5	80.3	2.2	53.6	6.7	39.3	0.3	0.1	
Spruce bark	23.4	73.4	3.2	53.6	6.2	40	0.1	0.1	19.5
Willow	15.9	82.5	1.6	49.8	6.1	43.4	0.6	0.06	18.3
Forest residue	16.9	79.9	3.2	52.7	5.4	41.1	0.7	0.1	19.2
Herbaceous and agricultural biomass									
Miscanthus grass	15.8	81.2	3	49.2	6	44.2	0.4	0.15	18.6
Reed canary grass	17.7	73.4	8.9	49.4	6.3	42.7	1.5	0.15	18.1
Sweet sorghum grass	18.1	77.2	4.7	49.7	6.1	43.7	0.4	0.09	18.2
Switchgrass	14.5	80.4	5.1	49.7	6.1	43.4	0.4	0.11	18
Barley straw	18.5	76.2	5.3	49.4	6.2	43.6	0.7	0.13	19
Wheat straw	18.1	74.8	7.1	49.4	6.1	43.6	0.7	0.17	18.1
Chicken litter	14.4	47.8	37.8	60.5	6.8	25.3	6.2	1.2	

*) Mass fraction in [%]

a) FC: fixed carbon

b) VM: volatile matter

c) Phyllis2 database for biomass and waste (mean value)

2.4 Biomass ash

Biomass and consequently biomass fuels contain inorganic matter. The inorganic materials can be separated into two broad categories: inherent and extraneous. Inherent inorganic material is part of the organic structure of the fuel and often exists in conjunction with oxygen-, sulfur- and nitrogen-containing functional groups. These functional groups can accommodate favorable locations for the inorganic component to be chemically associated in forms of cations and chelates. Additionally, inorganic matter can occur in a very fine particulate form within the organic structure behaving as an inherent constituent. Extraneous inorganic material originates from external sources. Harvesting, handling, processing, and storage of biomass fuels commonly leads to involuntary contaminations with soil or clay in the form of mineral particles, adding to the amount of inorganic matter in biomass fuels (Lackner, 2010).

The total amount of inorganic material is typically represented as the ash content of a biomass or biomass fuel. Different biomass fuels cover a broad range of ash content stretching from 0.5 % up to more than 12.0 % mass fraction on a dry basis. The ash content of some typical biomass fuels is listed in Table 2.2. Wood from forest trees, here as wood chips, typically has lower amounts of ash. Logging residues like bark locate in mid range and herbaceous crops like straw span towards the upper end.

Table 2.2: Ash content of different biomass fuels (van Loo & Koppejan, 2012)

Biomass fuels	**Ash content [%]***
Bark	5.0 - 8.0
Wood chips with bark (forest)	1.0 - 2.5
Wood chips without bark (forest)	0.8 - 1.4
Sawdust	0.5 - 1.1
Waste wood	3.0 - 12.0
Straw and cereals	4.0 - 12.0
Miscanthus	2.0 - 8.0
Olive residues	2.0 - 4.0

*) Mass fraction in percent (dry basis)

The chemical composition of the ash content in biomass fuels is important as it influences the ash behavior in combustion and gasification systems. The inorganic elements contained in the ash content of biomass, often referred to as main ash-forming elements, are: potassium (K), sodium (Na), calcium (Ca), magnesium (Mg), iron (Fe), aluminum (Al), silicon (Si), phosphorus (P), sulfur (S), and chlorine (Cl) (Lackner, 2010). These elements form different compounds depending on the temperature in the system and the relative amounts with respect to each other. The chemical ash composition of different biomass fuels, with the elements expressed as oxides, is shown in Table 2.3. The various compositions influence the melting point of a substance and can pose a problem regarding agglomeration, defluidization, deposit build-up, slagging, as well as fouling of fluidized-bed systems. One approach to reduce those problems is the implementation of fuel design.

Fuel design was developed primarily for biomass combustion to remedy operational issues that come with the implementation of biomass feedstock. It constitutes a general approach to fuel characterization and blending. The behavior of biomass ash in combustion and gasification processes is influenced by several factors such as ash composition, bed material, temperature and pressure in the system. These parameters impact ash transformation reactions that are responsible for the ash behavior under certain conditions. Temperature and pressure for a conversion process are often predetermined and the choice of implemented bed material is often governed by the primary conversion process, that is combustion or gasification, and various economic factors. However, the ash composition can be varied by blending different biomass fuels to achieve a favorable biomass ash composition in respect of certain ash transformation reactions (Boström et al., 2012), (Skoglund, 2014).

Thermo-chemical conversion processes like combustion and gasification yield two general ash fractions: fly ash and bottom ash. Fly ash is generated during combustion by volatilization of a fraction of the ash-forming compounds in the biomass fuel and releasing them into the gas phase. Upon release, they form very small primary particles, 5-10 nm in size, due to re-oxidation and subsequent nucleation reactions. These particles are transported with the flue gas and grow in size by coagulation, agglomeration and condensation to a particle size smaller than 1 µm. They represent the fine mode of fly-ash particles. Bottom ash is

Table 2.3: Chemical ash compositions as oxides of different biomass fuels (Vassilev et al., 2010)

Biomass fuels	SiO_2	CaO	K_2O	P_2O_5	Al_2O_3	MgO	Fe_2O_3	SO_3	Na_2O	TiO_2
Wood and woody biomass										
Birch bark	4.38	69.06	8.99	4.13	0.55	5.92	2.24	2.75	1.85	0.13
Pine bark	9.20	56.83	7.78	5.02	7.20	6.19	2.79	2.83	1.97	0.19
Poplar	3.87	57.33	18.73	0.85	0.68	13.11	1.16	3.77	0.22	0.28
Poplar bark	1.86	77.31	8.93	2.48	0.62	2.36	0.74	0.74	4.84	0.12
Spruce bark	6.13	72.39	7.22	2.69	0.68	4.97	1.90	1.88	2.02	0.12
Willow	6.10	46.09	23.40	13.01	1.96	4.03	0.74	3.00	1.61	0.06
Forest residue	20.65	47.55	10.23	5.05	2.99	7.20	1.42	2.91	1.60	0.40
Herbaceous and agricultural biomass										
Miscanthus grass	56.42	10.77	19.75	5.54	0.79	3.01	0.94	2.28	0.47	0.03
Reed canary grass	84.92	3.31	2.93	3.88	1.32	1.42	1.04	1.04	0.09	0.05
Sweet sorghum grass	66.85	10.41	9.49	3.47	0.81	3.12	0.58	3.47	1.74	0.06
Switchgrass	66.25	10.21	9.64	3.92	2.22	4.71	1.36	0.83	0.58	0.28
Barley straw	50.78	9.89	28.18	2.97	0.67	2.87	0.95	2.22	1.39	0.08
Wheat straw	50.35	8.21	24.89	3.54	1.54	2.74	0.88	4.24	3.52	0.09
Chicken litter	5.77	56.85	12.19	15.40	1.01	4.11	0.45	3.59	0.60	0.03

Values given as mass fraction in [%]

produced by non-volatile inorganic compounds remaining in the char. They may melt and coalesce inside and on the surface of the char depending on the temperature and chemical composition of the particles forming residual ash particles in the bed. Fluidized-bed system with relatively high superficial gas velocities can transport and entrain fractions of the residual ash representing the coarse fly-ash mode, typically larger than 5 µm (van Loo & Koppejan, 2012).

In DFB systems, described in section 2.1.1, the combustion and gasification units are usually spatially separated and bed material is circulated between them. Ash particles entrained with the flue gas from the combustion unit typically constitute coarse ash and fine ash. Coarse ash particles are bigger particles that can be separated from the flue gas stream by gravitational separators and are recirculated back into the combustion reactor. The fine ash particles are transported to the flue gas filters, where they become separated from the gas stream and eventually removed from the system. Small biomass particles that are entrained from the DFB gasification unit with the product gas stream are referred to as fly coke. The fly coke particles can be described as particles with higher amounts of unconverted carbon. Fly coke is separated in the product gas filters and nowadays recirculated to the combustion unit in the DFB system as it contains unburnt carbon. The carbon-rich fly coke could also be discharged of the process and used as biochar in different applications e.g. soil amendment, carbon sink, or water retention (Kuba, 2016).

2.5 Interaction of biomass ash and bed material with focus on different interaction mechanisms

Section 2.2 described different bed materials implemented in bench-scale as well as industrial-scale fluidized-bed systems, and gave an overview of the advantages and problems that arise due to the interaction of biomass ash and bed material. This interaction can lead to the formation of layers on the surface of the bed particles. Those layers can have a positive effect on the process performance and the products e.g. reducing the formation of tars during gasification. On the other hand, the interaction can have a negative effect on the system causing agglomeration problems, deposit build-up, and eventually defluidization. To minimize unwanted problems and emergency shutdowns of power plants, and study layer formation to the advantage of process improvement, it is important to understand the interaction between biomass ash and bed material. The interaction is governed by different mechanisms that primarily depend on the existing biomass ash composition and the bed material involved. This chapter describes the distinct mechanisms responsible for layer formation and agglomeration problems in fluidized-bed systems.

Quartz sand

The appearance of layers and agglomration problems were first recognized with quartz sand as bed material. The turbulent conditions in a fluidized bed were reported to create collisions between bed material particles and ash particles. Contact between such particles could lead to attachment of the ash particles to the bed material surface forming a coating layer (Valmari et al., 1999). Similar bed material surface coatings on quartz sand were reported by Öhman & Nordin (2000). Thermodynamic equilibrium calculations with the prerequisite of bed material/ash interaction acknowledged the formation of coated layers, but no mechanism was proposed (Zevenhoven-Onderwater et al., 2001).

Brus et al. (2003) investigated the formation of those layers on quartz bed particles during full-scale combustion and reported that the initial growth rate of the coating layers was approximately a few micrometers per day, decreasing over time. Visser et al. (2004) found

that the coating thickness increased over time and with increasing ash content of the fuel. Subsequent investigations with controlled fluidized-bed agglomeration tests (CFBA) showed layers with similar appearance and determined that the initiating step for the layer formation is the reaction of gaseous alkali with the surface of the quartz bed particles (Öhman et al., 2005). The free silica of the quartz particles was attacked by the alkali from the gas phase forming low-melting potassium (K)-silicates on the quartz particle surface. Therefore, the initiating step for layer formation on quartz particles was identified as a gas-solid reaction between the gaseous alkali and the free silica of quartz particles. Additionally, the presence of low-melting K-silicates on the particle surface was found to subsequently promote an inward attack of calcium (Brus et al., 2005).

Further investigations regarding the mechanism of layer formation on quartz particles also suggested the formation of low-melting K-rich silicates due to the reaction of potassium with the quartz particle as the initiating step. Thereafter, coarse fly ash containing calcium attaches to the surface and partly dissolves into and reacts with the K-silicate melt. The diffusion of calcium into the molten phase and gradual formation of high-temperature melting calcium (Ca)-silicates, followed by the precipitation of these more stable Ca-silicates, lead to the formation of a homogeneous Ca-rich inner layer on the particle. Simultaneously, an outer layer is formed resembling the composition of the biomass ash. The inner layer growth rate diminishes over time as the calcium concentration increases in the inner layer. Additionally, the diffusion of calcium into the layer leads to the release of potassium (K) out of the layer, which reduces the amount of molten phase in the inner layer. Both, the reduced amount of molten phase due to expulsion of potassium and the increasing calcium concentration are responsible for reduced inner layer growth over time. The thickness of the heterogeneous outer layer is reduced over time (He et al., 2014).

Quartz bed particles of different ages exhibit differences in layer morphology and layer composition which lead to a more detailed investigation of the layer growth rates over time. Particles with less than 24 hours of operational time experienced slow layer growth followed by faster layer growth for particles between 1 and 14 days of operation. The high layer growth rate depleted over time and continued to much lower growth rates for particles with

more than 2 weeks of operation. Results showed that the layer growth for particles less than 1 day is accelerated because of the K-rich silicate melt that prompts the diffusion of Ca into the layer. Hence, the layer growth process is reaction and diffusion controlled in K-rich silicate melt as the main crystalline phase. For middle-aged particles (1 to 14 days of operation) the layer formation is diffusion controlled resulting in medium layer growth rates while no melt exists in the layer. The main crystalline phase appeared to be Ca_2SiO_4. Older quartz particles (more than 14 days of operation) experience low inner layer growth rates due to higher diffusion resistance resulting from a thicker and denser layer (He et al., 2016).

Olivine

Olivine has been found to influence tar reduction during biomass gasification attributed to the iron (Fe) and magnesium (Mg) content (Nordgreen et al., 2006a), (Nordgreen et al., 2006b). It is commercially used as bed material in various industrial fluidized-bed systems.

Layer formation on olivine particles appears to be significantly different compared to layer formation on quartz particles. Kirnbauer & Hofbauer (2011) found an inner more homogeneous layer and an outer layer on the olivine particle. The inner layer was dominated by calcium silicates, with the magnesium (Mg) and iron (Fe) content decreased compared to unused olivine. The outer layer, also Ca-rich, resembled more the composition of fine ash and its main ash elements Ca, Mg, Si, and O. The inner layer appeared to be growing into the particle, the outer layer growing outward from the particle. The prefered formation of calcium silicates compared to potassium silicates resulted in a low concentration of potassium in the layers. Elevated potassium content inside the olivine particle is caused by the high volatility of alkali components at combustion and gasification temperatures. Similar results were found by Grimm et al. (2011). Experiments on the interaction of miscanthus ash and olivine found corresponding layer compositions (Kaknics et al., 2016).

Long-time experiments to study the layer formation on olivine over time helped to identify a possible layer formation process. It is significantly different to the layer formation of quartz particles. The composition of the first visible layer formed on olivine bed particles shows increased amounts of calcium (Ca) and no potassium (K). The initial step of layer forma-

tion on olivine particles is based on a solid-solid interaction between CaO and olivine. This solid-solid reaction is suggested to be a substitution reaction where Ca^{2+} is embedded into the crystal structure of olivine. For the calcium (Ca^{2+}) ion to be incorporated into the structure, either an iron (Fe^{2+}) ion or a magnesium (Mg^{2+}) ion has to be expelled. Additionally, ash-forming elements from the biomass fuel can produce low-melting K-silicates. These K-silicates may act as an adhesive between the olivine particle and the biomass ash representing an intermediate that facilitates the substitution reaction (Kuba et al., 2016b).

Feldspar

Industrial-scale fluidized-bed systems often use natural sand as bed material containing mostly quartz sand. Part of the natural sand mixture are non-quartz mineral particles. The dominating minerals in the non-quartz sand fraction are potassium (K)-feldspar and plagioclase (see feldspar description in section 2.2).

K-feldspar and plagioclase were first tested separately for their agglomeration behavior in a CFBA experiment by De Geyter et al. (2007). Three different fuels were used: bark, olive residue, and wheat straw. Bark was chosen to represent woody biomass with a high calcium (Ca) content, olive residue as a potassium (K) rich fuel, and wheat straw as biomass fuel with high potassium (K) and silica (SiO_2) content.

The combustion of wheat straw defluidized the K-feldspar bed after 2 hours into the experiment. SEM/EDS analysis showed no coating formation on the bed material and no agglomeration necks were found. Olive residue combustion with K-feldspar lasted 5.5 hours before the bed defluidized. A continuous layer formed on K-feldspar with a thickness of approximately 3 µm. The thin layer on K-feldspar was either due to the reduced combustion time until defluidization or a limited interaction potential between the fuel-ash alkali and the K-feldspar particles. Bark combustion lasted the scheduled 40 hours. A continuous layer with a thickness of approximately 3 µm was formed on the K-feldspar. An inner and outer layer could be determined.

Wheat straw combustion with plagioclase also defluidized the bed after 2 hours. No coating layer was formed and only some agglomerate necks were found with a composition dom-

inated by Si and K, as well as some Mg and Ca accumulated. Olive residue combustion lasted the scheduled 40 hours with plagioclase as bed material. Continuous layers were formed on plagioclase with a thickness of approximately 14 µm. A homogeneous inner layer and heterogeneous outer layer could be detected for plagioclase. Bark combustion endured the 40 hours as well. Plagioclase developed a continuous layer of approximately 4 µm. The layer could be determined as a homogeneous inner layer and a more heterogeneous outer layer.

Interactions between feldspar and biomass ash in a commercial DFB plant in Senden, Germany, have been reported regarding problems with deposit build-up and slagging behavior in zones of high temperatures as it is the case for the cyclone and postcombustion chamber. Feldspar particles were introduced as impurities of the logging residues into the gasifier. As part of the fuel feedstock, the impurities are mixed with the primary bed material olivine and act as bed material as well (Kuba et al., 2015).
These impurities have been further studied regarding their suitability in DFB systems. As part of the bed material samples, K-feldspar is one material of the impurites next to quartz sand, and was further examined to gain first insights into the mechanism of layer formation on K-feldspar particles and the thermal stability when interacting with biomass ash in continuous operation. Analyses regarding K-feldspar particle and layer morphology revealed a rather uniform appearance. The brighter layer on the slightly darker feldspar particle is shown in Figure 2.9. No visible inner or outer layer could be determined and no significant signs of crack development or layer breakage were found.

The particle layer composition was determined by several elemental spot analyses along a line from the feldspar particle (site x_1) towards the layer surface (sites x_2-x_9). An example of the spot analysis can be seen in Figure 2.10 (left) with the average values of multiple analyses depicted in a graph (right). A gradual reduction of silicon, potassium, and aluminum and a concurrent increase of calcium towards the layer surface can be observed. The autors conveyed also attention towards the increase of calcium inside the particle, where no distinguishable layer can be detected in the image (sites x_1-x_3). This calcium increase on the inside of the particle and the further increase towards the layer surface was observed

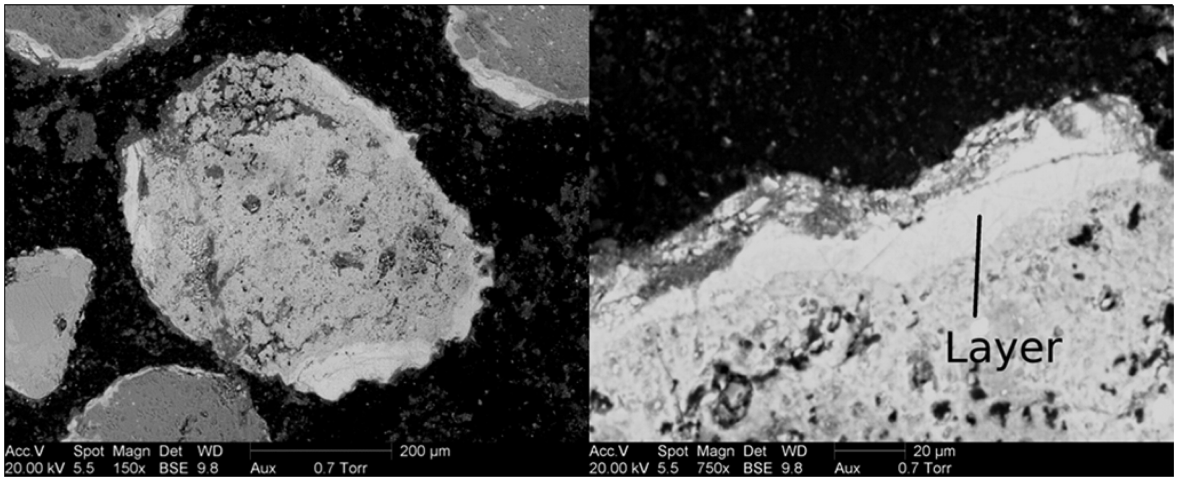

Figure 2.9: Typical cross-sections of K-feldspar layers on a particle (left) and a close-up (right) as observed by Kuba et al. (2016c)

on all K-feldspars that had developed a particle layer. The Ca increase coupled with the decrease of K may be caused by replacement of K and incorporation of Ca into the crystal structure. This suggests a substitution mechanism for layer formation on K-feldspar particles that preserves a stable crystal structure (Kuba et al., 2016c).

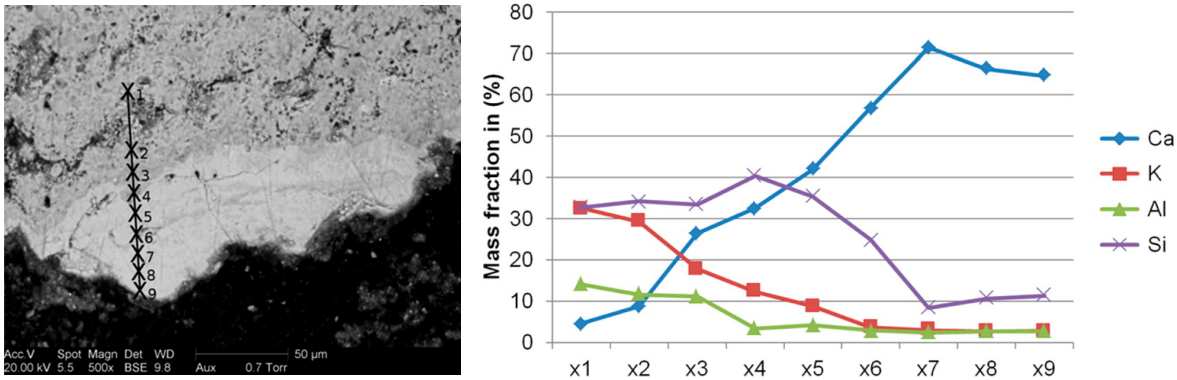

Figure 2.10: Elemental spot analysis along the cross-section of a K-feldspar layer (left) and averaged main components (C- and O-free basis) in the layer (right) as observed by Kuba et al. (2016c)

However, the proposed substitution mechanism has yet to be explained in detail. The ions involved in the mechanism have different charges. The potassium ion (K^{1+}) has a lower charge than the calcium ion (Ca^{2+}). Therefore, a simple substitution mechanism of K^{1+} with Ca^{2+} seems unlikely in respect of the charge difference. Instead, a coupled ion substitution mechanism is suggested for the layer formation on K-feldspar. The mechanism appears to

be connected with the release of potassium (K) from the particle itself, but no information has been gained so far regarding the involvement of other ions in the mechanism (Kuba, 2016).

The investigation of impurities like K-feldspar in DFB gasification with woody biomass as fuel feedstock only shows tendencies regarding the interaction of biomass ash and K-feldspar. The accumulated impurities in the fluidized-bed next to the primary bed material olivine behave as bed material as well, but they remain a very small fraction in terms of the total amount of bed material in the system. The composition of the small fraction of biomass ash interacting with the impurities may be influenced by interactions of the biomass ash and the primary bed material. This could influence the layer formation and layer characteristics of the impurities to a certain extent. Therefore, only general information and tendencies are gained from the investigation of layer formation on the impurities.

Furthermore, the biomass ash composition of woody biomass represents only a selected ash composition with high amounts of calcium (Ca), and medium amounts of silicon (Si), and potassium (K). This presents a limitation to the gained information as the obtained results cannot be simply transferred to other biomass fuels. Biomass fuels different from woody biomass, yield significantly different ash compositions. This needs to be considered when a transition to lower-cost biogenic biomass takes place. As an example, Skoglund (2014) investigated the behavior of phosphorus (P)-rich biomass and found that phosphorus is inclined to form compounds with alkali (K, Na) and alkaline earth metals (Ca, Mg). Therefore, phosphorus influences ash transformation reactions significantly and in turn the interaction of biomass ash and bed material as well. Added to that, the suggested coupled ion substitution mechanism for layer formation on K-feldspar involves calcium and potassium for which the phosphorus has an affinity to form compounds.

2.6 Aim of work

To investigate the interaction of K-feldspar with biomass ash compositions different from woody biomass, the use of low-cost biogenic biomass can be an advantage. Straw is characteristic for its high potassium (K) and silicon (Si) content, and chicken litter for its high calcium (Ca) and phosphorus (P) content. Straw has little calcium in the biomass ash present which brings up the question if the use of straw can contribute to layer formation on K-feldspar, bearing in mind that calcium would be needed for the proposed coupled ion substitution mechanism. Furthermore, the influence of phosphorus can be evaluated by producing fuel blends of straw and chicken litter. This lead to the investigation of fuel blends with straw and chicken litter about their performance in fluidized-bed combustion systems and layer formation on K-feldspar.

3 Materials and Methods

3.1 Raw materials and fuel pellets

3.1.1 Raw materials

The raw materials used for the fuel mixtures were chicken litter and straw, shown in Figure 3.1. Chicken litter originated from a laying hens farm in Styria, Austria, where chicken manure gets locally dried and pelletized with sustainable energy and sold as fertilizer without additives. Straw was aquired from an animal feed plant in Upper Austria, Austria. The raw material straw pellets were a pelletized mixture of coarse fibers of wheat straw and barley straw.

Figure 3.1: Pre-pelletized raw materials straw (left) and chicken litter (right)

3.1.2 Fuel mixtures

Three different fuel mixtures were prepared for the fluidized bed experiments: one fuel mixture comprising only straw, one mixture with a content of 10 % chicken litter and 90 % straw, and one mixture consisting of 30 % chicken litter and 70 % straw (with % notation as mass fraction in percentage dry mass). For easier referencing within this thesis, you may also find the fuel mixtures described and abbreviated as Straw, Chicken Litter Low (CLL) and Chicken Litter High (CLH), respectively.

The duration of the fluidized bed experiment for each fuel mixture was set to last for 40 hours, hence, a continuous fuel feed for that period was required. Additionally, in case a rerun of the experiments were necessary and for future agglomeration tests, sufficient amount of fuel had to be provided. Our estimates showed roughly 100 kg of each fuel mixture would be reasonable. The fuel mixtures were prepared manually. To simplify the handling of approximately 300 kg of fuel in total, the raw materials were weighed and mixed together in batches of 25 kg. Moreover, the preparation of smaller batches and the manual mixing process already ensured initial homogenization of the fuel mixtures before pelletization.

3.1.3 Fuel pellets

As described by Kaltschmitt et al. (2009), the pelletization process of biomass and the quality of the produced fuel pellets is mainly influenced by the particle size and form of the raw materials, the water content, and the temperature of the material during pelletization. The raw materials were pelletized, thus, already had the right size and form for the pelletization of the fuel mixtures. As stated by Kaltschmitt et al. (2009), a good pellet quality can be achieved with a water content of 10-15 %. Analyses of the raw material pellets for their water content showed chicken litter had approximately 11 % and straw had approximately 9.4 % water content. The water content would be further reduced during the pelletization process due to mechanical heat generated by friction in the pelletizer. As a result, approximately 2 liters of water were added to each 25-kg batch of fuel mixture, raising the water content of each batch to roughly 18 % before pelletization.

The pellets were produced with the flat die pelletizer PP200 (Cissonius GmbH), as shown in Figure 3.2. The die diameter was 200 mm and the holes diameter was 6 mm. The horizontally rotating die was powered by a heavy current electric motor and the two compression rollers were mounted on a static single shaft centered above the die. The gap between the die and the rollers could be adjusted via screws on the outside of the machine by raising or lowering the single shaft. As the die was rotating and the material between the die and the rollers created resistence, the compression rollers started turning because of friction. The fuel mixtures were fed manually with a bucket from above through a funnel onto the flat die. The material on the die was continuously pressed into the holes of the die and eventually emerged on the lower side of the die where the compressed material was cut into pellets by a metal blade. After cutting, the pellets left the pelletizer via a shute and were collected in a bucket.

Figure 3.2: Flat die pelletizer PP200, die diameter 200 mm, holes diameter 6 mm (Cissonius GmbH)

To produce pellets with high durability, 4-5 pelletization cycles were necessary. In the first cycle, the prepelletized raw materials in the fuel mixtures were broken apart between the rollers and the die. The loose material went through the die without sufficient compression and showed no sign of stability when leaving the die on the bottom. Additionally, the material had already warmed up due to mechanical heat generated by friction. Water vapour was visibly forming above the die, therefore reducing the water content in the mixture. The loose material was collected and fed again into the pelletizer. In the following cycles, the water

content was gradually reduced and the compactness of the material further increased. After the second cycle, some of the material had already the form of pellets, but showed no sign of hardness. The pellets could be easily squashed with the fingers or would break apart by falling into the collection bucket. After the fourth cycle, the hardness of the pellets had significantly increased and could be broken apart with fingers only by applying great strength. After the fourth or fifth cycle, the pellets had sufficient durability. The surface of the pellets had a glassy appearance, indicating sufficient compression, and were impossible to break apart by hand. The pellets still hot from the last cycle had to be cooled and further dried. Since we chose perfectly sunny weather conditions in September to do the pelletization outside, the pellets were spread on large plastic sheets on the ground. About two hours were enough to cool the pellets down and further dry them under the sun. Analyses of the finished fuel pellets showed the following water content: Straw 9.1 %, Chicken Litter Low 8.8 %, and Chicken Litter High 9,6 %. Figure 3.3 shows an example of the fuel pellets produced of the fuel mixture Chicken Litter High (CLH). The pellets were approximately 1.0-1.5 cm long and had a diameter of about 6 mm.

Figure 3.3: Produced fuel pellets of the fuel mixture Chicken Litter High (CLH)

3.2 Bench-scale fluidized-bed reactor

The three combustion experiments were conducted in a bench-scale (5 kW) bubbling fluidized-bed (BFB) reactor, as shown in Figure 3.4. The reactor has been previously described in

detail by Öhman & Nordin (1998). The stainless-steel reactor had a total height of 2 meters and was insulated to reduce heat loss and facilitate uniform temperature conditions. To ensure steady temperatures along the axis of the reactor, electrical heaters were used in the freeboard section. The cross-section of the fluidized bed had an inner diameter of 100 mm and of the freeboard 200 mm. The bottom of the fluidized-bed was an air distribution plate made of perforated stainless steel. The air distributor had evenly distributed holes spread across the surface with a total open area of about 1 %. Temperature and pressure in the bed could be monitored continuously with two thermocouples and two pressure probes. The fuel pellets were stored in a fuel bunker with a maximum capacity of about 15 kg. The fuel bunker was mounted on a vibrating plate and equipped with a screw conveyor. The fuel feed was controlled by both the rotation velocity of the screw and the vibration intensity of the bunker. The bunker vibration also prevented the possible appearance of bridging effects in the pellet packing. The fuel pellets fell through a chute directly onto the fluidized bed in the reactor. The used bed material was K-feldspar with a grain size of 200-250 µm. 540 g of K-felspar were initially set as bed material for the experiments. The fluidized bed was maintained with a primary air flow of 50 NL/min through the distribution plate from below the bed. The primary air velocity was approximately six times the minimum fluidization velocity which translates to about 0.6 m/s. A secondary air flow of 30 NL/min introduced into the reactor above the fluidized bed provided sufficient oxygen to ensure complete combustion of the generated gases. The temperature measurements were established with type N thermocouples. It has to be noted that the primary air preheater and the propane feed were not used during the experiments.

3.3 Bed material sampling, deposition probe, ash sampling, particulate matter, and flue gas analysis

Bed material samples were taken during the combustion experiments after 2 hours, 4 hours, and 8 hours. The samples were taken with a self-made device, essentially mimicing a small cyclone separator. The inlet duct of the cyclone was an extended tube with about

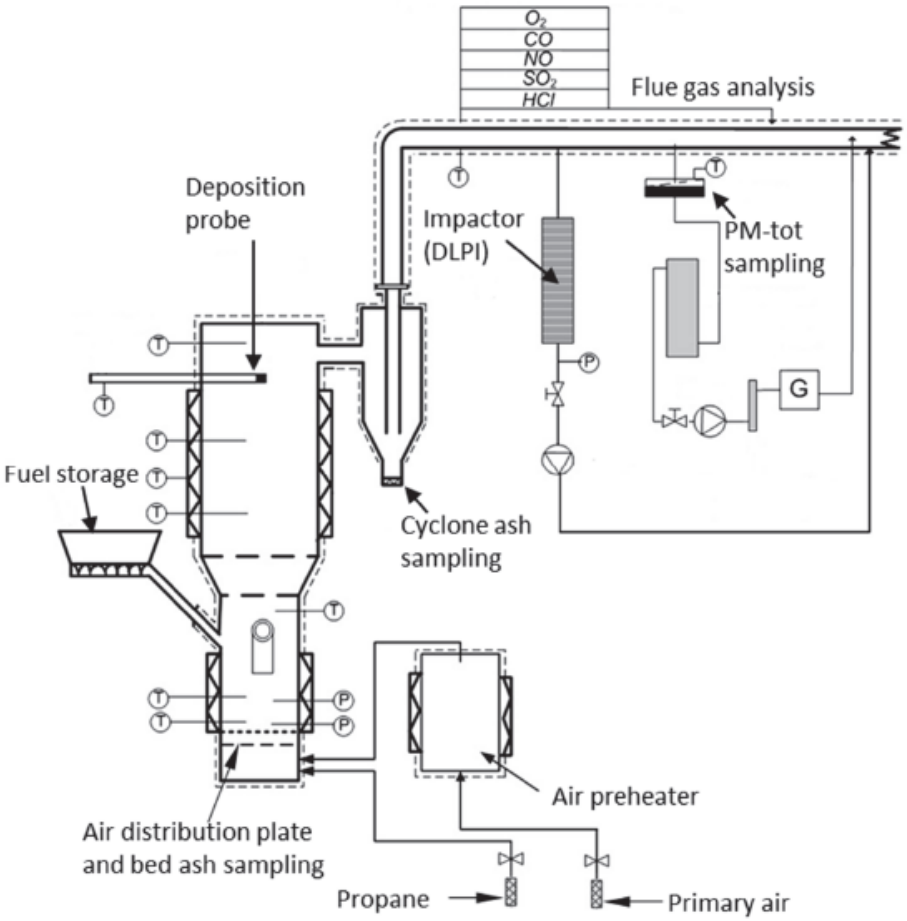

Figure 3.4: Schematic illustration of the bench-scale bubbling fluidized-bed reactor with sampling arrangement (Skoglund, 2014, p. 7)

one centimeter in diameter that could be manually inserted into the reactor down to the fluidized bed through a sampling pipe. The sampling pipe was permanently integrated in the reactor design and could be temporarily opened to take bed samples. The immersion tube of the cyclone was attached to the suction unit of an industrial vacuum cleaner that provided the necessary pressure difference to extract bed material from the fluidized bed. The bed material sample was transported with the gas flow through the inlet duct to the cyclone where it was separated from the gas flow. The material outlet was at the bottom of the conical section of the cyclone where a tin can was held in place to collect the hot bed sample. The bed material sampling required great caution and appropriate safety protection equipment as hot gases and hot bed material were handled. Bed samples were also taken

after defluidization of the fluidized bed when the reactor was cooled down and opened.

An air-cooled deposition probe with stainless steel test rings was used to collect deposit samples in the freeboard section. The metal test ring should simulate super heater tube surfaces and the surface temperature was measured with thermocouples. A controlled flow of cooling air on the inside of the test ring regulated the temperature of the metal test ring. During all combustion experiments, the ring surface temperature was set to 450 °C and the exposure time was scheduled with 6 hours during steady operation conditions.

After the freeboard section of the reactor, the flue gas passed through a cyclone separator with a cut size of >10 µm (PM_{10}). The cyclone ash collected in the bottom of the cyclone could be extracted through opening the bottom section by removing a sealing plug.

The ash particles not separated from the flue gas by the cyclone separator were analyzed by isokinetic particulate matter (PM) sampling. To determine the mass size distribution of the ash particles, a 13-step low-pressure cascade impactor from Dekati, Ltd. (DLPI) was used. The impactor classifies the size of ash particles according to their aerodynamic diameter in the range of 0.03-10 µm. Aluminum foils, not greased, were used as substrates in the impactor, and the impactor was heated to about 150 °C during the sampling.

Total particulate matter mass concentrations were measured through isokinetic sampling from the flue gas at approximately 160 °C using traditional equipment with quartz fiber filters.

The concentration of CO, SO_2, and HCl was continuously monitored during the combustion experiments using Fourier transform infrared spectroscopy (FTIR).

3.4 Determination of ash content and ash composition of the fuel feedstock

Ash content

The determination of the ash content of the fuel feedstock was conducted according to DIN EN 15403 ‘Solid recovered fuels - Determination of ash content’. The norm provides

guidance to determine the mass of inorganic residue remaining after ignition of a fuel under specified conditions. The result is the ash content on a dry basis expressed as mass fraction in percent of the dry matter in the fuel. The fuel sample was placed on a dish, oven-dried at a temperature of 105℃ and weighed. Next, the sample was put into the cold furnace and the temperature was raised evenly to a temperature of 250℃ over a period of 50 min. The temperature was maintained at that level for 60 min to allow the volatiles to leave the sample before ignition. Then, the temperature was further raised evenly to 550℃ over a period of 60 min and kept at that level for 120 min. This should have ensured complete incineration of the biomass fuel sample and transformed the sample completely to ash. The dish with the ash was removed from the furnace and allowed to cool to ambient temperature in a desiccator without desiccant. The ash content was then determined by weighing and calculation. Two determinations were carried out for each fuel sample.

Ash composition

An X-ray fluorescence spectrometer was used to determine the ash composition of the fuel feedstock. The ash samples from the above described determination of ash content were melted in a Merck Spectromelt at 1050℃ and placed on a stainless-steel plate at a temperature of 400℃. The XRF analysis was performed with a PANalytical Axios Advanced analyzer. The analyzer was equipped with a rhodium anode and works in a vacuum. An excitation voltage of 50 kV and a tube current of 50 mA were applied. XRF analysis is a bulk analysis of the sample, hence, the results showed the elemental composition of the total ash sample. The results were expressed in oxides of the corresponding elements. The obtained results were subsequently converted to the actual content of the elements as opposed to their oxides, and also further converted to mole/kg fuel for easier visualization as a so called fuel fingerprint.

3.5 SEM-EDS analysis of the bed samples

The bed material samples were mounted in epoxy, sanded and polished. Scanning electron microscopy (SEM) in conjunction with energy-dispersive X-ray spectroscopy (EDS) was used to determine the elemental composition and morphology of the bed particles.

Quantitative line scans were used to determine the element distribution along a line from the inside of the original bed particle to the surface of the particle. The line scans were used to determine the element distribution of the layers formed on the bed particles during the combustion experiments. Multiple line scans were obtained across the surface of the analyzed bed particles to ensure data collection from various sites on a particle.

Additionally, element mappings were carried out for the bed samples. An element mapping provides an image showing a two-dimensional spatial distribution of elements in a sample. The image is produced by progressively rastering the electron beam point by point over a selected area. The resolution is determined by the beam size, and the relative response is determined by the actual element concentration and the duration of the beam in one point. Element mappings are often displayed in false color. In the element mappings obtained from the analysis, each element was represented by an automatically assigned color and the element concentration in one point was represented by the brightness of that color. Brighter areas represented a higher element concentration, whereas darker areas represented a lower element concentration. The detected elements could be displayed separately by individual element maps or assembled in one layered element map only showing the elements with the highest concentration in the analyzed area. Both, layered element maps and individual element maps were used to analyze the bed material samples. For the layered element maps, a larger area was predominantly selected to cover several bed particles simultaneously in one image. This helps to distinguish between bed particles with different elemental compositions, that is, between feldspar and impurities like quartz sand particles. Layered element maps are an advantage, expecially as the back-scattered electron (BSE) images display different morphologies with a range of hues of the color grey. The individual element maps predominantly covered only one bed particle at a time to produce an image

with higher resolution compared to the layered element maps. The individual element maps of single bed particles were used to determine the composition of the formed layers quantitatively. Layer formation on bed particles was indicated on the individual element mappings by brighter areas along the outline/surface of a bed particle for certain elements. In the case of feldspar, the formation of a Ca-layers was expected in some sort of interaction with the elements K, Mg, Si, P, and S. That way, Ca-layers on feldspar particles could be identified qualitatively by analyzing the individual element map of calcium. Brighter areas (layers) around the outline of a feldspar particle indicated higher concentrations of calcium, hence, potential layer formation.

4 Results

This chapter provides initial results for the combustion experiments with fuel mixtures of chicken litter and straw. The initial results comprise analyses of raw materials, fuel mixtures, bed materials, and the temperature and pressure profiles of the fluidized bed in the reactor.

4.1 Raw materials

The raw material analyses of straw, chicken litter, conifer bark, and pine bark are shown in Table 4.1. Listed are the total ash content and the content of main ash-forming elements as mass fraction in percentage on a dry basis. Straw and chicken litter are the two raw materials utilized for the combustion experiments in this thesis. Pine bark is merely mentioned for comparison, whereas conifer bark was implemented as a raw material in subsequent experiments undertaken in the same fluidized bed reactor. The combustion experiments with conifer bark are not described within this thesis.

Skoglund (2014) argues for another useful way to visualize the inorganic content of a fuel - a fuel fingerprint - in respect of reaction paths, ash chemistry and transformation processes, and eventually, fuel design. Displaying the inorganic content in units of mol/kg allows for an easy and prompt comparison of elements in the raw materials and later in the fuel mixtures. Figure 4.1 presents the content of the main ash-forming elements in straw, chicken litter, conifer bark and pine bark, and can be considered a fuel fingerprint. Total Ca/(K+Na) molar ratios of the raw materials are: 0.23 for straw, 1.64 for chicken litter, 1.87 for conifer bark, and 1.20 for pine bark.

Table 4.1: Total ash content and the content of main ash-forming elements in the raw materials

	Straw	Chicken litter	Conifer bark	Pine bark
Ash	6.42	24.61	5.88	6.13
K	0.65	1.36	0.16	0.11
Na	0.12	0.80	0.17	0.081
Ca	0.20	4.57	0.85	0.31
Mg	0.17	1.53	0.25	0.084
Fe	0.081	0.14	0.26	0.34
Al	0.052	0.20	0.33	0.43
Si	1.83	0.65	1.04	1.72
P	0.076	3.42	0.079	0.038
S	0.14	0.76	0.049	0.036
Cl	0.23	1.01	0.035	0.020

Values given as mass fraction in percent (dry basis)

4.2 Fuel mixtures

The raw material analysis of straw and chicken litter (Table 4.1, Figure 4.1) regarding their total ash composition was the starting point for the applied fuel design strategy. The presentation of the inorganic elements in units of mol/kg are more favorable compared to other ways as they allow an atom-per-atom comparison of the elements (Skoglund, 2014). The main ash-forming elements were grouped forming positively charged metal ions acting as Lewis acids (K, Na, Ca, Mg, Fe, Al) and negatively charged molecular (Si, P, S) or atomic ions (Cl) acting as Lewis bases. The relative concentrations of these elements in the raw material ashes were used to determine the different fuel blends for the experiments. Fundamental knowledge of the ash transformation reactions was helpful to determine the theoretical fuel blends. The total ash content and the content of main ash-forming elements in the fuel pellets are displayed in Table 4.2 and as a fuel fingerprint in Figure 4.2. Particular consideration was given to the elements K, Ca, Si, and P during the development of the fuel blends as they play a major role concerning agglomeration and layer formation on different bed materials. Total Ca/(K+Na) molar ratios are: 0.34 for Straw, 0.75 for Chicken Litter Low, and 1.35 for Chicken Litter High.

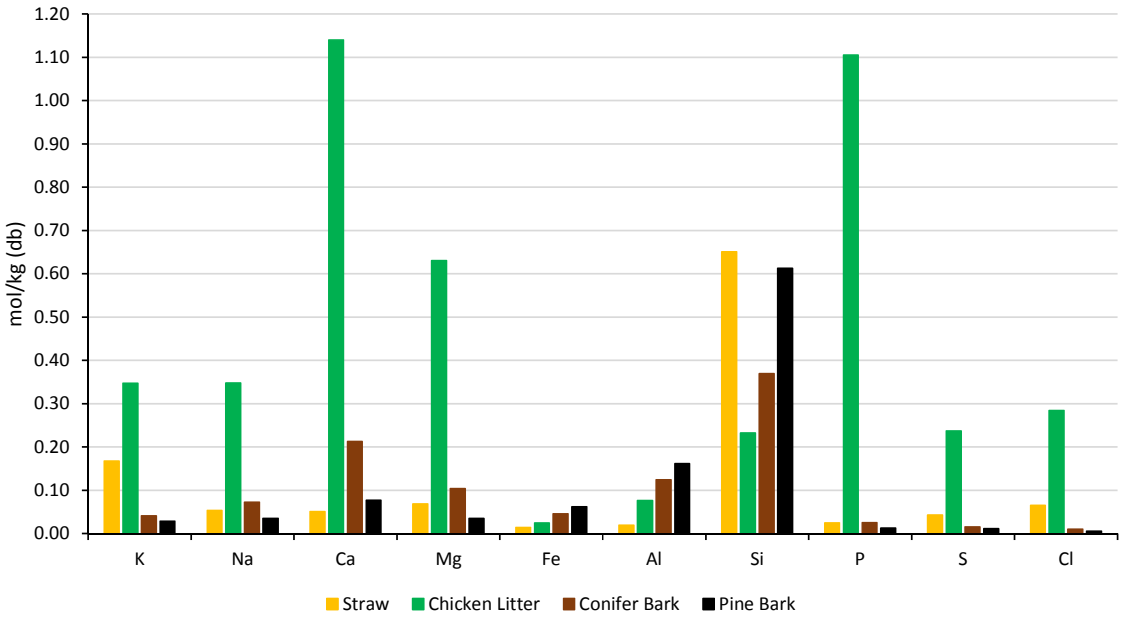

Figure 4.1: Content of the main ash-forming elements in units of mol/kg for the following raw materials: straw, chicken litter, conifer bark, and pine bark

The fuel mixture Straw was produced by pelletization of the pre-pelletized raw material wheat straw and therefore has similar biomass ash composition as the raw material. The composition of the raw material was received upfront from the wheat straw producer which explains the small difference in biomass ash composition between raw material and fuel pellets. Straw is characterized as high in potassium (K) and silicon (Si), and low in calcium (Ca). The molar K/Ca ratio is 2.65 for the fuel pellets. High amounts of potassium have been shown problematic for fluidzed-bed operations because of melt-induced agglomeration. The total ash amount of 6.92 % mass fraction is the lowest of the three fuel mixtures.

Chicken Litter Low is the fuel mixture comprising 90 % wheat straw and 10 % chicken litter to combine the biomass ash composition of the two raw materials. The addition of 10 % chicken litter raised the total ash content for CLL to 8.81 % mass fraction. The increase is attributed to the ash from pure chicken litter with a total ash amount of 24.61 % mass fraction. Therefore, a small amount of chicken litter added, increases the ash fraction of the fuel mixture significantly. The content of K and Ca in the biomass ash was nearly balanced for CLL with a molar K/Ca ratio of 1.17. The silicon content remained fairly constant.

Table 4.2: Total ash content and the content of main ash-forming elements in the pelletized fuel mixtures

	Straw	Chicken Litter Low	Chicken Litter High
Ash	6.92	8.81	13.09
K	0.87	1.14	1.43
Na	0.050	0.094	0.20
Ca	0.34	0.99	2.46
Mg	0.077	0.16	0.38
Fe	0.074	0.086	0.092
Al	0.10	0.12	0.16
Si	2.05	1.98	1.92
P	0.062	0.25	0.75
S	0.13	0.16	0.24
Cl	0.025	0.037	0.077

Values given as mass fraction in percent (dry basis)

Chicken Litter High as the fuel mixture of 70 % wheat straw and 30 % chicken litter significantly changed the ash composition. The total ash content of 13.09 % is the highest of the three experiments. The K content further increased gradually, whereas the Ca content increased significantly leading to a molar K/Ca ratio of 0.60 in CLH. Additionally, a significant increase for the phosphorus (P) and magnesium (Mg) content was established, possibly influencing the ash behavior as explained by Skoglund (2014). Phosphorus will be further addressed in the discussion about layer formation.

4.3 Combustion experiments

This section describes the upper bed and lower bed temperature and pressure profiles registered during the combustion experiments with Chicken Litter High, Chicken Litter Low and Straw. The heating and cooling phases of the reactor are not shown as no significant information can be optained from their visualization. The time axis in the figures represents the actual clock time during which the experiments were carried out. The left ordinate represents the temperature of the upper and lower bed, whereas the right ordinate represents

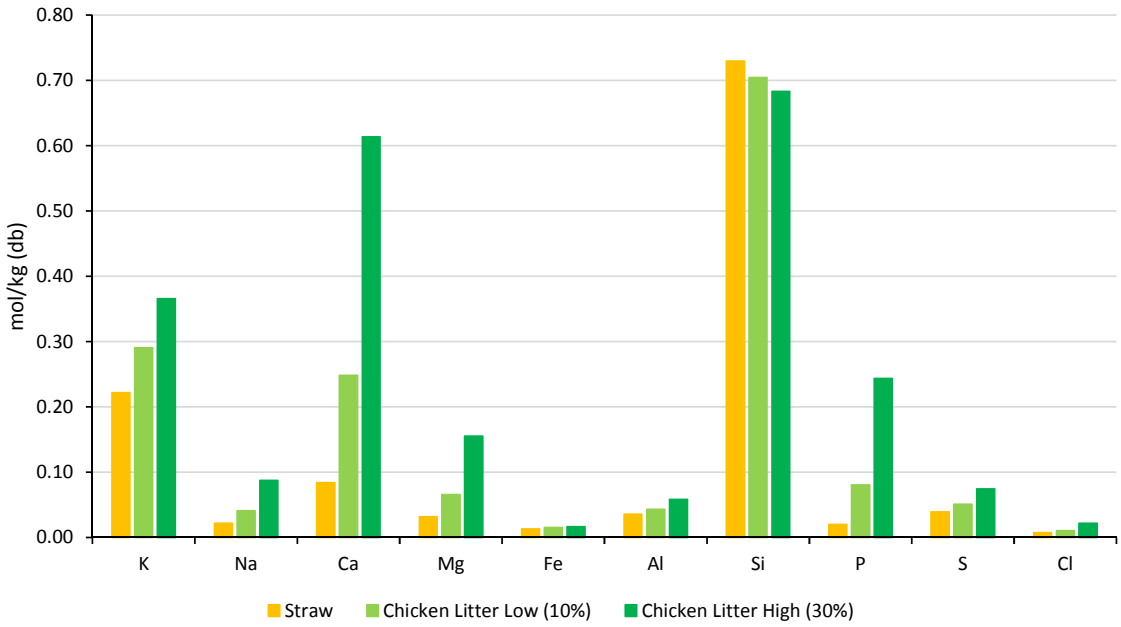

Figure 4.2: Content of the main ash-forming elements in the fuel mixtures in units of mol/kg

the pressure in the upper and lower bed. Throughout the experiments, the upper bed temperature was on average 1.5℃ lower than the lower bed temperature. Therefore, the upper bed temperature is the reasonable temperature information to describe the bed temperature characteristics for the experiments. The combustion experiments were planned to endure a total duration of 40 hours to observe initial layer growth mechanisms on the feldspar bed material. As the results show, all three experiments defluidized under 10 hours of operation.

Combustion of Chicken Litter High

Figure 4.3 shows the temperature and pressure profiles registered during the combustion experiment with Chicken Litter High. The fuel feed was started at 3.15 pm when the fluidized bed in the reactor had reached a temperature of about 560℃ with the first pellet dropping into the reactor 3 minutes later at 3.18 pm. The first pellet in the reactor marked the start of the experiments elapsed time.

During the first 75 minutes, the upper and lower bed temperature gradually increased due to combustion of the CLH fuel pellets in the reactor. To ensure conditions for combustion in the reactor the temperature for the fluidized bed was aimed at 780-800℃. During the exper-

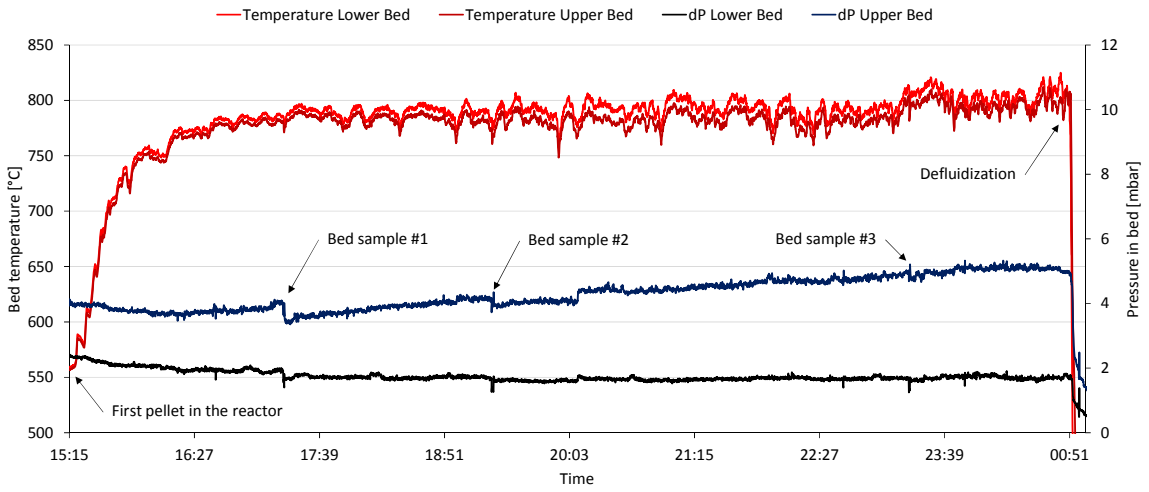

Figure 4.3: Bed temperature and pressure profiles for the combustion experiment with Chicken Litter High

iment an average upper bed temperature of 785 °C was provided by controlling the fuel feed and the heating elements in the freeboard section. At around 11.15 pm, 8 hours of elapsed time, the upper bed temperature was elevated to an average of 795 °C with maximum temperatures occasionally reaching 805 °C for the remaining time of the experiment. At 0.15 am, 9 hours 32 minutes of elapsed time, bed defluidization occured at an upper bed temperature of 806 °C. The fuel feed was immediately stopped and the heating elements turned off.

The upper and lower bed pressure, specifically the difference between them, is an indicator for the amount of material in the fluidized bed. The smallest difference in the beginning is reasonable, as there is only bed material present in the fluidized bed. After the start of the fuel feed the pressure difference gradually increased due to the fuel pellets introduced into the bed material and the amount of ash accumulating in the fluidized bed over time. The observable steps or spikes in the pressure lines are the results of sample extractions from the fluidized bed as indicated for the three bed samples. In particular, the pressure difference immediately before and after the bed sample extraction changed. The bed samples required a certain amount of material to be extracted from the fluidized bed, that is, bed material and ash, thus reducing the amount of material in the fluidized bed. This is reflected in the reduced pressure difference after the sample extraction. Defluidization was shown in the immediate collapse of the pressure difference indicated in the far right of the diagram. Bed

material and ash formed agglomerates, and the fluidizing air became to weak to maintain the bed.

The experiment with Chicken Litter High as fuel feedstock defluidized after 9h 32min. During this period, a total of 6.94 kg of fuel pellets were introduced into the reactor with an average fuel feed rate of 0.73 kg/h. A constant feed rate was ensured to provide continuous and steady operation conditions. The total ash content of CLH was 13.09 % mass fraction. Hence, the total amount of biomass ash produced in the reactor by combusting the 6.94 kg fuel was approximately 0.91 kg. The amount of bed material in the beginning of the experiments was 0.54 kg K-feldspar. As a result, significant amounts of biomass ash were in the fluidized bed next to the initially set up bed material.

Combustion of Chicken Litter Low

Figure 4.4 shows the temperature and pressure profiles registered during the combustion experiment with Chicken Litter Low. The fuel feed was started at 8.46 am when the fluidized bed in the reactor had reached a temperature of about 560℃ with the first pellet dropping into the reactor 2 minutes later at 8.48 am. The first pellet in the reactor marked the start of the experiments elapsed time.

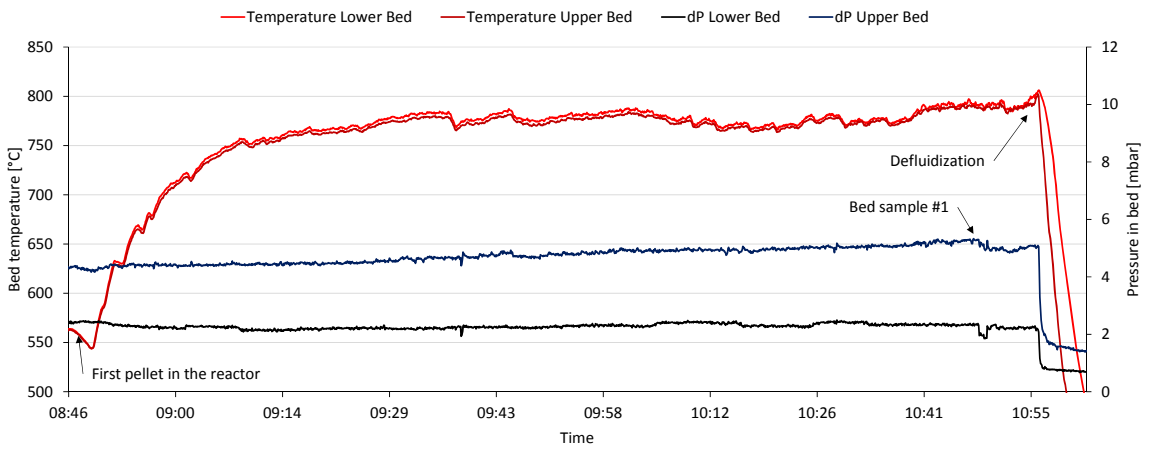

Figure 4.4: Bed temperature and pressure profiles for the combustion experiment with Chicken Litter Low

The initial drop of the upper and lower bed temperature is a result of the fuel feed start and the fuel pellets falling into the reactor bed while simultaneously lowering the temperature

of the bottom heat element in the freeboard. The heat elements temperature was reduced to prevent a temperature overshoot of the bed above the aimed temperature interval of 780-800 °C. The bed temperature started to increase when sufficient heat was generated by combustion of the fuel pellets. After 47 minutes of elapsed time the bed temperature reached 780 °C for the first time. From that point onwards, the average upper bed temperature was 774 °C over the next 65 minutes until 10.40 am, that is, 1 hour 52 minutes elapsed time. For the last 17 minutes of the experiment the average upper bed temperature was 788 °C. At 10.57 am, 2 hours 9 minutes elapsed time, bed defluidization occured with a maximum upper bed temperature of 802 °C.

The upper and lower bed pressure difference gradually increased over time during the experiment with the only two noticable disturbances for the deposition probe placement and the bed sample extraction as indicated in the diagram. Bed defluidization is indicated with the collapse of the pressure difference as shown on the right end of the diagram.

The experiment with Chicken Litter Low as fuel defluidized significantly earlier, after about 2h 9min. A total of 1.53 kg fuel pellets was fired in the reactor with an average fuel feed rate of approximately 0.68 kg/h up to the point of defluidization. The total ash content of CLL was 8.81 % mass fraction which leads to a total amount of 0.13 kg biomass ash produced in the reactor.

Combustion of Straw

Figure 4.5 shows the temperature and pressure profiles registered during the combustion experiment with Straw. The fuel feed was started at 8.39 am when the fluidized bed in the reactor had reached a temperature of about 470 °C with the first pellet dropping into the reactor 3 minutes later at 8.42 am. The first pellet in the reactor marked the start of the experiments elapsed time.

The temperature aim for this experiment was 730-750 °C. In the first 33 minutes the upper bed temperature increased to 710 °C. To introduce more fuel and therefore ash into the system before agglomeration occured, the average upper bed temperature was 712 °C for the next 90 minutes until 10.45 am, or 2 hours 3 minutes elapsed time. After that, the upper

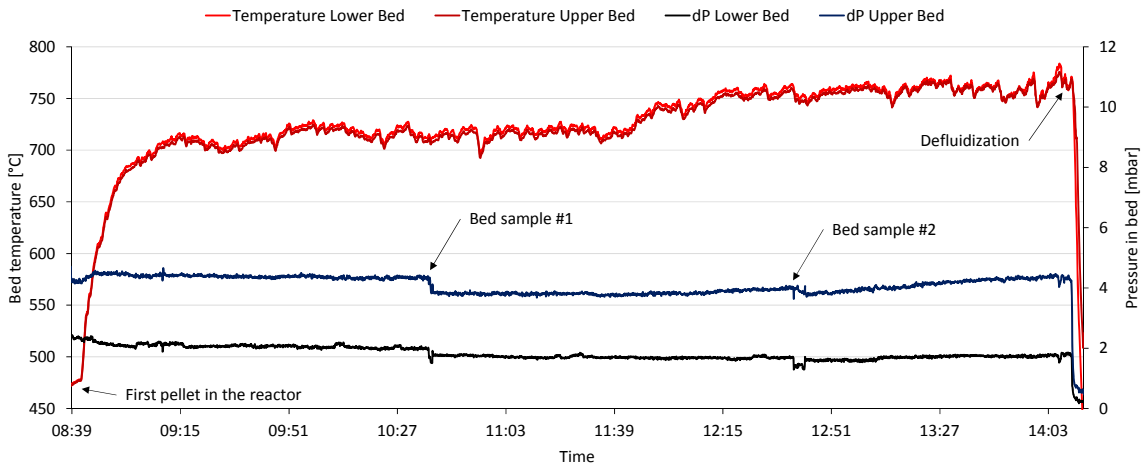

Figure 4.5: Bed temperature and pressure profiles for the combustion experiment with Straw

bed temperature was gradually elevated to a temperature of about 750 ℃ over the course of the next 30 minutes until 12.15 pm. For the remaining time, the average upper bed temperature was 752 ℃. About 4 minutes before defluidization the upper bed temperature had a maximum of 776 ℃. At 2.11 pm, 5 hours 29 minutes of elapsed time, defluidization occured at a temperature of 768 ℃.

The difference of upper and lower bed pressure gradually increased over time between bed sample extractions and deposition probe placement. The steps in the relatively continuous pressure lines are the result of bed sample extractions. The pressure difference is reduced as the amount of material in the fluidized bed was reduced by the samples taken. At the far right of the diagram at around 2.07 pm, 4 minutes before defluidization, both pressure probes recorded a pressure disturbance indicating signs of defluidization. The dynamic in the bed probably broke apart initial agglomerates and a fluidized bed was maintained for a couple more minutes until the bed finally defluidized at 2.11 pm. The time where the initial defluidization signs occured correlates with the maximum temperature reached 4 minutes before defluidization.

The experiment with Straw as fuel feed defluidized after about 5h 29min. The combustion of straw at temperatures of approximately 780-800 ℃ generates problematic low-melting biomass ash and poses a significant agglomeration risk in fluidized beds. Thermodynamic

equilibrium calculations with FactSage provided information regarding the melting temperature of biomass ash from straw. The temperature aimed for during combustion experiments with straw was 730-750 ℃, therefore lower compared to the experiments with CLH and CLL (780-800 ℃). The reactor burned approximatly 3.29 kg of fuel pellets with an average fuel feed rate of 0.6 kg/h. The total ash content of Straw was determined at 6.92 % mass fraction resulting in a total of 0.23 kg of biomass ash produced in the reactor.

4.4 Elemental compositions of the bed material samples for fresh and used feldspar particles

Figure 4.6 shows the results of the XRF analyses for fresh feldspar and used feldspar from the combustion of Chicken Litter High (CLH), Chicken Litter Low (CLL) and Straw. The samples of used feldspar were taken after bed defluidization and cooling of the bed. The result of an XRF analysis shows the calculated elemental composition of the total sample. That allows for a general comparison of the content of the main ash-forming elements in the bed material samples.

For fresh feldspar, the main elements are potassium (K), silicon (Si) and aluminum (Al) as shown in Figure 4.6. The concentration of the remaining elements in fresh feldspar can be interpreted as mere traces of the elements or not present at all, since the detected concentration is very low compared to the three main elements. The used feldspar samples from the combustion experiments of Straw and Chicken Litter Low show nearly the same concentration for potassium (K), silicon (Si) and aluminum (Al) as the fresh feldspar, but already indicate a slight increase for the concentration of calcium (Ca). In contrast, the used feldspar from the Chicken Litter High combustion experiment shows a significant decrease for the concentrations of potassium (K), silicon (Si) and aluminum (Al), and a significant increase of calcium (Ca). The concentrations of K, Si and Al are about halfed compared to fresh feldspar, whereas Ca can be detected in a substantial amount. Furthermore, phosphorus (P) and sulfur (S) concentrations are elevated.

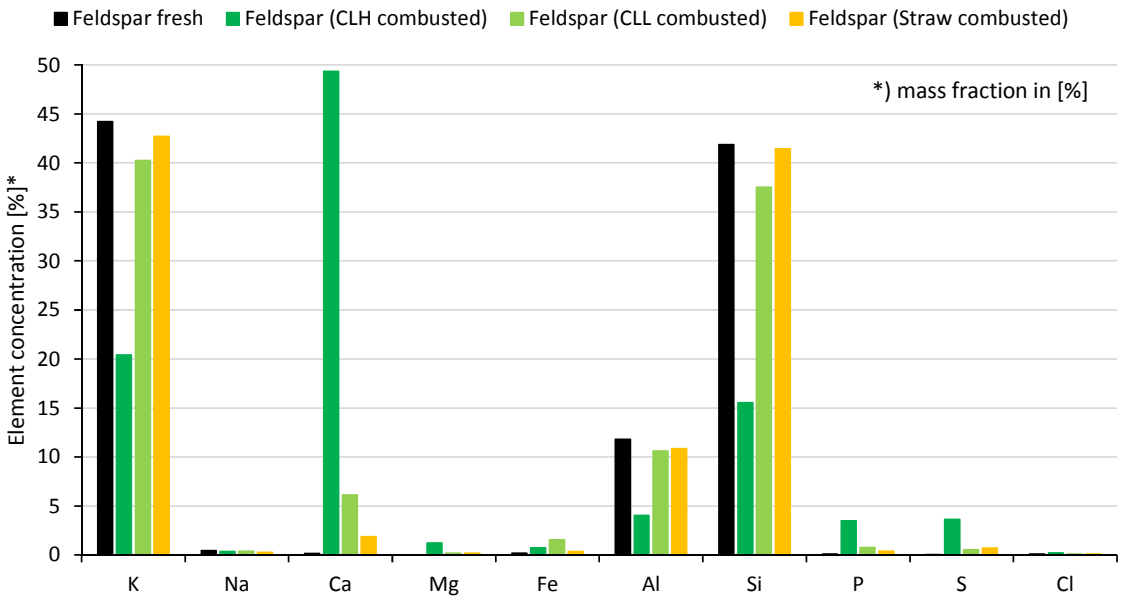

Figure 4.6: XRF analyses of the bed materials: fresh feldspar and used feldspar from the combustion of CLH, CLL, and Straw after defluidization

4.5 Bed particle layer formation and morphology

The bed material samples taken during the combustion experiments and after bed defluidization were analyzed with SEM-EDS and the initial results are illustrated in this section. It should be noted in advance that a comprehensive statistical analysis of the formed layers was not possible with the initial results and a qualitative approach towards layer characterisation was implemented instead. The selected images in this section show the morphology of the bed particles and the corresponding elemental mappings primarily for calcium to determine qualitative layer formation on the bed particles. Additionally, data obtained by line scans is given to establish the initial layer thickness and the composition of the layer.

4.5.1 SEM-EDS analysis of the bed material from the combustion of Chicken Litter High (CLH)

Bed sample after 2 hours

Figure 4.7 shows the scanning electron microscopy (SEM) image and the calcium (Ca) mapping of a bed particle from the bed sample taken 2 hours into the combustion experiment. The left SEM image also depicts the locations of multiple line scans taken with the SEM-EDS analysis. The data evaluation for the line scans 66 to 74 showed a single Ca peak of 0.9 At% in line scan 66. The right calcium mapping shows a thin non-continuous layer along the outline of the bed particle, indicating higher amounts of calcium. Line scan 76 from a different bed particle not depicted here also showed a single Ca peak of 1.1 At%.

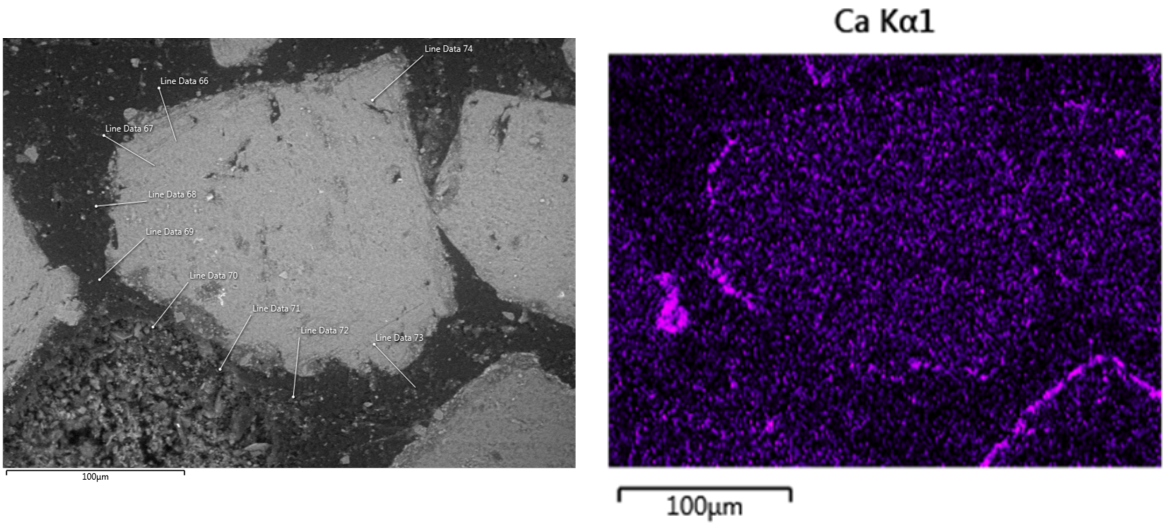

Figure 4.7: Scanning electron microscopy (SEM) image and calcium (Ca) mapping of the bed sample after 2 hours in the combustion of Chicken Litter High

Bed sample after 4 hours

Figure 4.8 shows the scanning electron microscopy (SEM) images and the calcium (Ca) mappings of two bed particles from the bed sample taken 4 hours into the combustion experiment. On both SEM images on the left are the line scan locations indicated for the line scans 41 to 58.

For the top particle, line scan 45 registered a 0.7 µm calcium layer with approximately 1.7 At% Ca and possibly a slight potassium (K) decrease in the same location. Line scan 49 registered a 1.0 µm calcium layer with approximately 1.4 At% Ca, and line scan 50 detected a single Ca peak of approximately 1.2 At%. Additionally, line scan 57 from the bottom particle registered a 4.0 µm calcium layer with a maximum calcium concentration of approximately 1.8 At% and a noticable reduction of potassium (K) in the same location. The line scans 53, 56 and 58 detected single Ca peaks with approximately 0.9 At%, 1.1 At% and 1.2 At%, respectively. Additional line scans from a third bed particle not shown in Figure 4.8 registered the following: line scan 59 showed a 0.9 µm calcium layer with about 1.5 At% Ca, line scan 61 registered a single Ca peak of 1.1 At% and line scan 65 a single Ca peak of 0.9 At%.

The top right-hand calcium mapping already shows indications of a continuous calcium layer forming along the outline of the particle with only a couple of smaller gaps in between. Additionally, on the bottom calcium mapping of the other particle, a continuous calcium layer can be noticed along the particle outline.

Bed sample after 8 hours

Figure 4.9 shows the scanning electron microscopy (SEM) images and the calcium (Ca) mappings of two bed particles from the bed sample taken 8 hours into the combustion experiment. The bottom SEM image on the left indicates the line scan locations for the line scans 24 to 29.

For the bottom row particle images, the line scans 24 and 26 presented a 2.4 µm calcium layer of 1.6 At% and a 1.0 µm calcium layer of 1.8 At%, both with a possible indication of reduced potassium (K) in that region. Furthermore, line scans 25, 27 and 28 displayed a single Ca peak of 1.4 At%, 1.1 At% and 1.2 At%, respectively. The line scans 35 and 37 of a fourth bed particle not depicted here, revealed a short section of a 1.0 µm calcium layer with 1.3 At% and a single Ca peak of 0.9 At%.

For the big bed particle in the middle of Figure 4.10, a phosphorus mapping is included next to the SEM image and Ca mapping. The line scans 19 and 20 show a 1.0 µm calcium layer

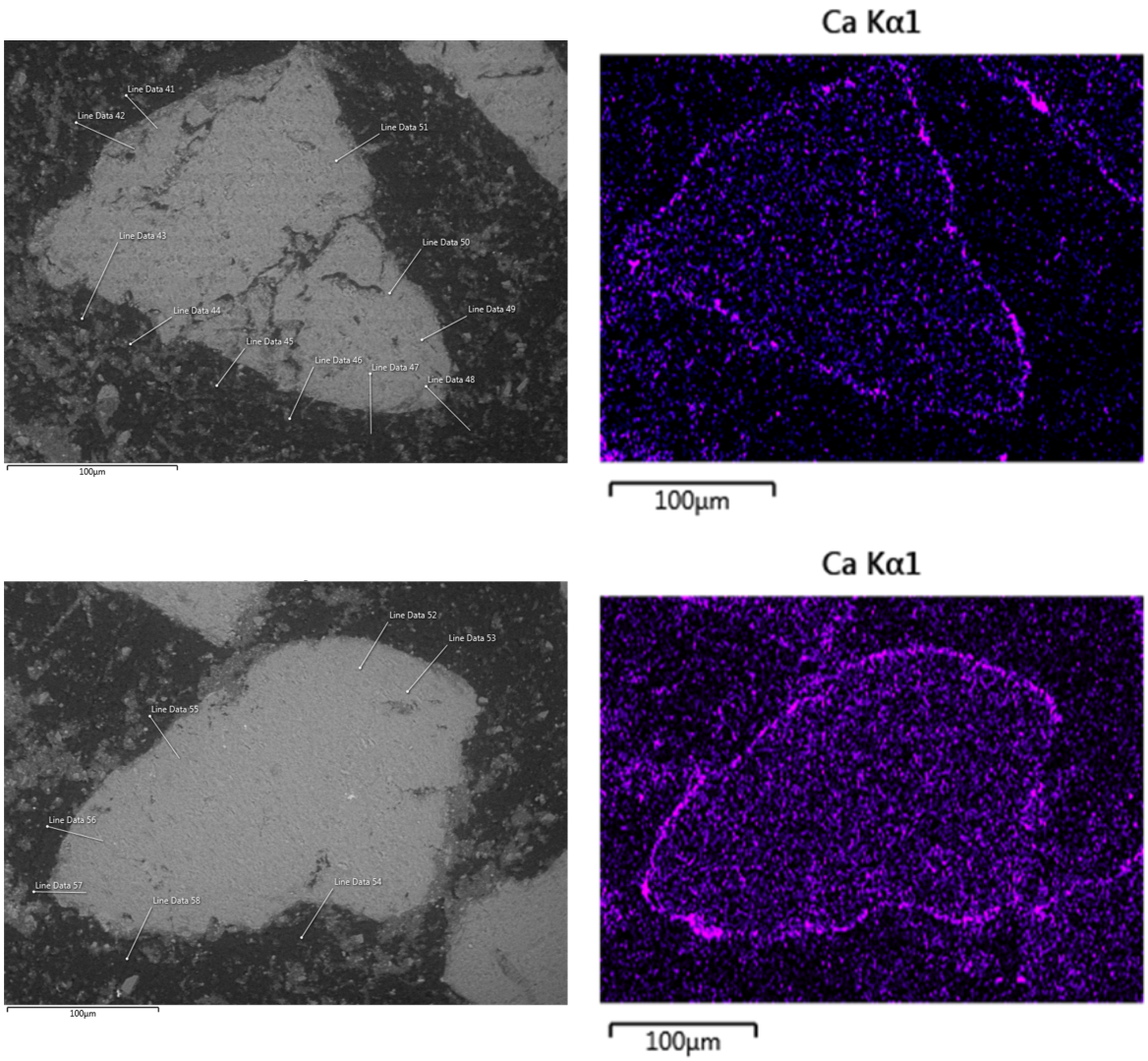

Figure 4.8: Scanning electron microscopy (SEM) images and calcium (Ca) mappings of the bed sample after 4 hours in the combustion of Chicken Litter High

of 1.3 At% and 1.5 At%, respectively. In addition to that, a single phosphorus (P) peak with 0.8 At% was detected in line scan 19. Furthermore, line scan 23 displayed a single Ca peak of approximately 0.9 At%. The qualitative layer of calcium shown along the outline of the bed particle overlaps with the qualitative layer of phosphorus, which is harder to determine than the calcium layer.

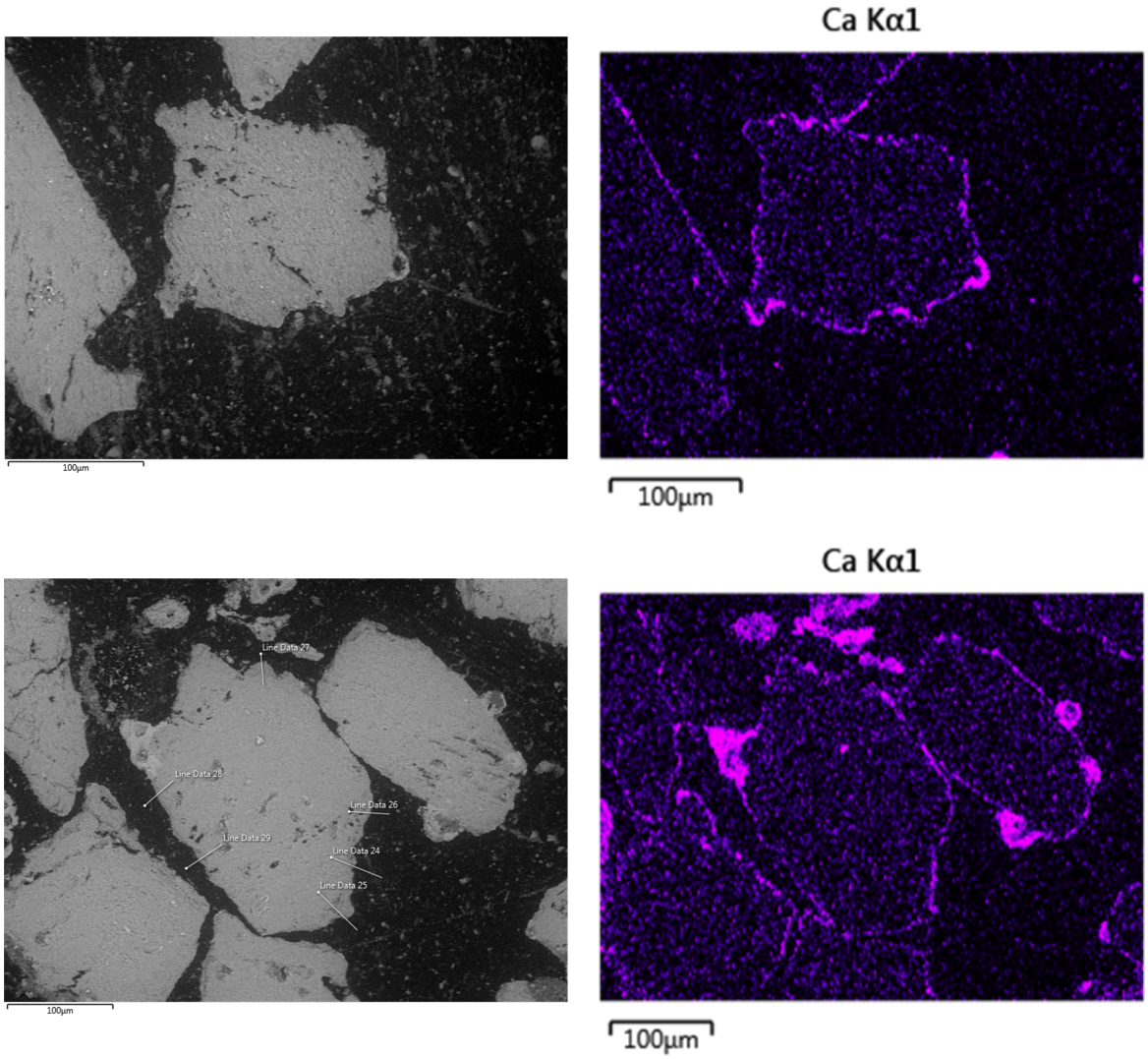

Figure 4.9: Scanning electron microscopy (SEM) images and calcium (Ca) mappings of the bed sample after 8 hours in the combustion of Chicken Litter High

Bed sample after defluidization (9h 32min)

Figure 4.11 shows the scanning electron microscopy (SEM) image and the calcium (Ca) mapping of a bed particle from the bed sample taken after bed defluidization. The SEM image on the left indicates the line scan locations for the line scans 9 to 17.

Line scans 10 and 11 detected a 0.7 µm calcium layer of 2.0 At% and a 0.8 µm calcium layer of 3.2 At%, respectively, both possibly indicating reduced potassium (K) concentration at the locations. In addition, line scans 13, 14, 15 and 17 showed single Ca peaks of

4.3 At%, 1.6 At%, 1.3 At% and 1.1 At%.

The calcium mapping on the right shows a continuous layer of Ca around the outline of the bed particle.

4.5.2 SEM-EDS analyses of the bed material from the combustion of Chicken Litter Low (CLL) and Straw

The combustion experiment with Chicken Litter Low has defluidized shortly after 2 hours and the SEM-EDS analysis of bed material particles shows no signs of any form of layer formation. Therefore, no SEM images or element mappings are included for this experiment as no valuable information can be gained from them.

Figure 4.12 shows samples of the bed material from the experiment with Straw after 4 hours of operation. The SEM images (left), layered element mappings (center) and calcium mappings (right) show that the feldspar bed material has no qualitative layer formed along the outline of the bed particles. The layered element mappings in the center help to distinguish between quartz and feldspar particles. Quartz is depicted as the red and lime green colored areas representing the elements silicon (Si) and oxygen (O), forming SiO_2. Potassium (K)-feldspar particles are displayed as the light blue and blue areas, representing potassium (K) and aluminum (Al) in the feldspar which is generally expressed as the chemical formula $KAlSi_3O_8$.

Consider the three bottom pictures in Figure 4.12 for a more detailed description. The center image represents the layered element mapping that shows a quartz particle in the top center of the image. The same particle in the right-hand calcium mapping shows a vague qualitative calcium layer around the outline of that particle. Such a layer is not visible on the feldspar particles in the same calcium mapping. The top row pictures also show four quartz particles (red/green) with other feldspar particles around (blue). The quartz particle farthest to the right is shown via a magnification in Figure 4.13.

This magnified quartz particle (Figure 4.13) in the middle of the images already has a qualitative layer forming on the particle outline, whereas the two feldspar particles extending into the images in the top and bottom right corner show no signs of a qualitative calcium layer. A comparison of the calcium and potassium mappings of the middle quartz particle reveals a higher concentration of potassium than calcium in the layer.

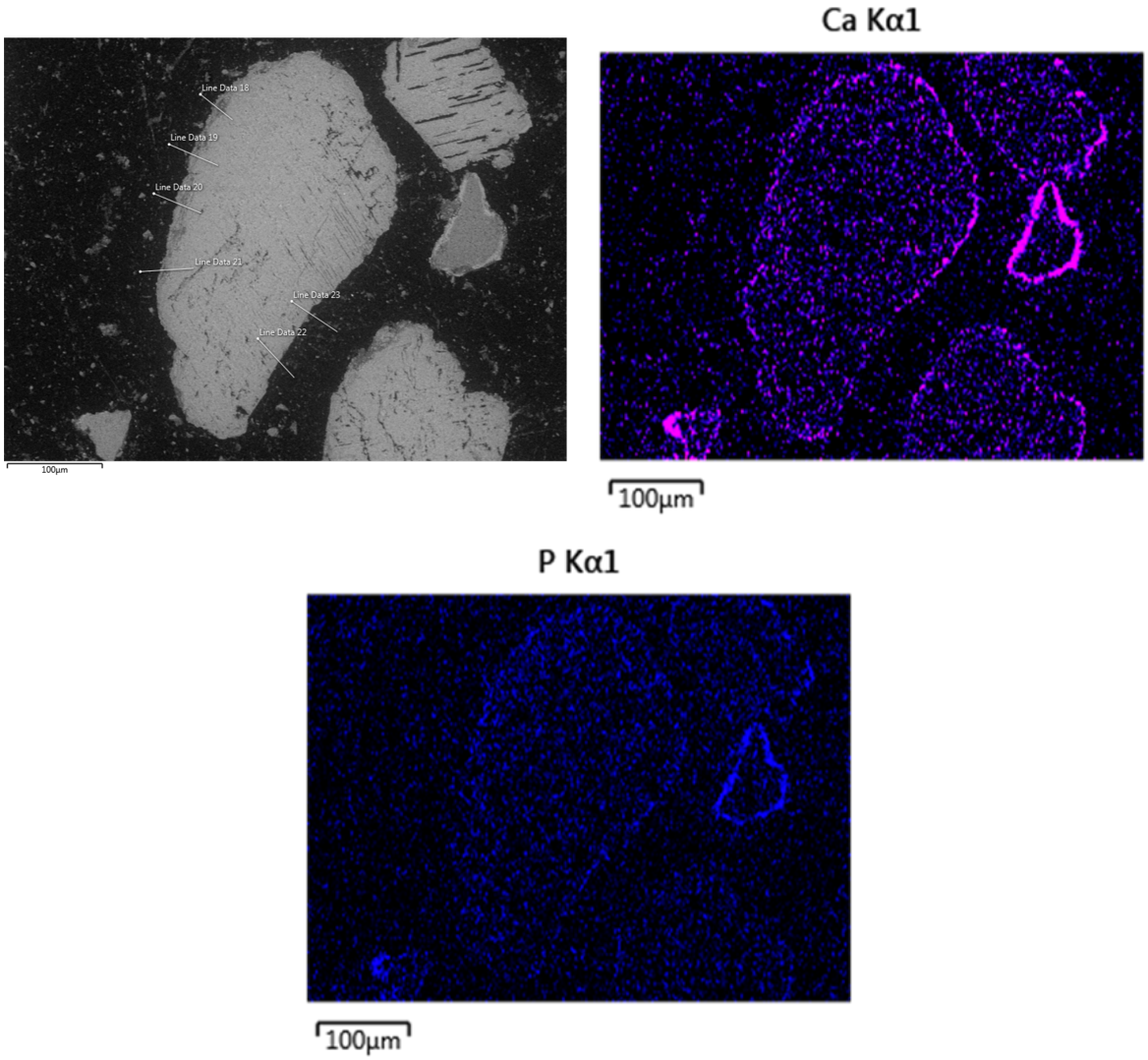

Figure 4.10: Scanning electron microscopy (SEM) image, calcium (Ca) mapping and phosphorus (P) mapping of a bed particle after 8 hours in the combustion of Chicken Litter High

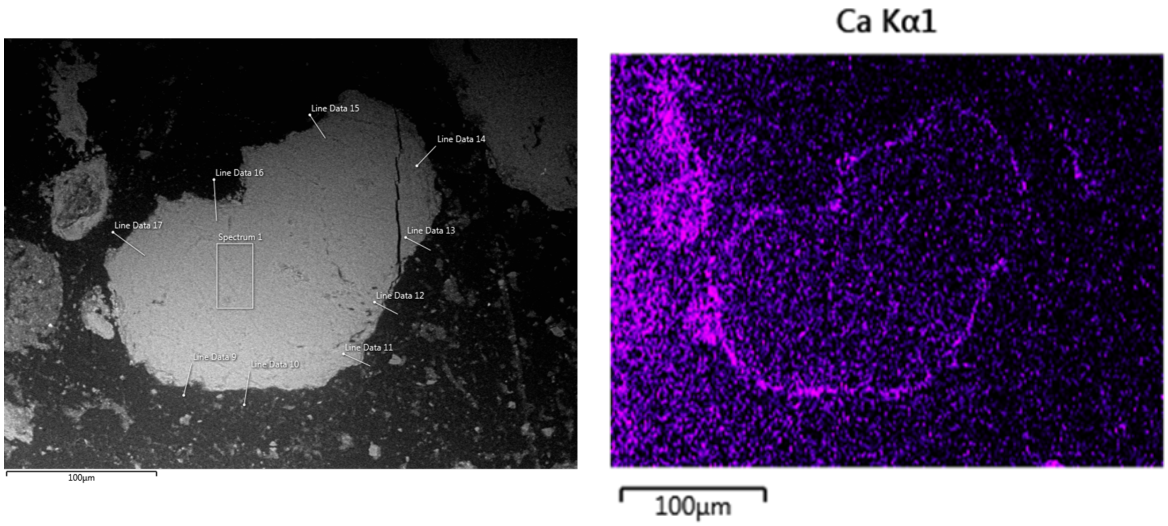

Figure 4.11: Scanning electron microscopy (SEM) image and calcium (Ca) mapping of the bed sample after defluidization (9h 32min) of the combustion of Chicken Litter High

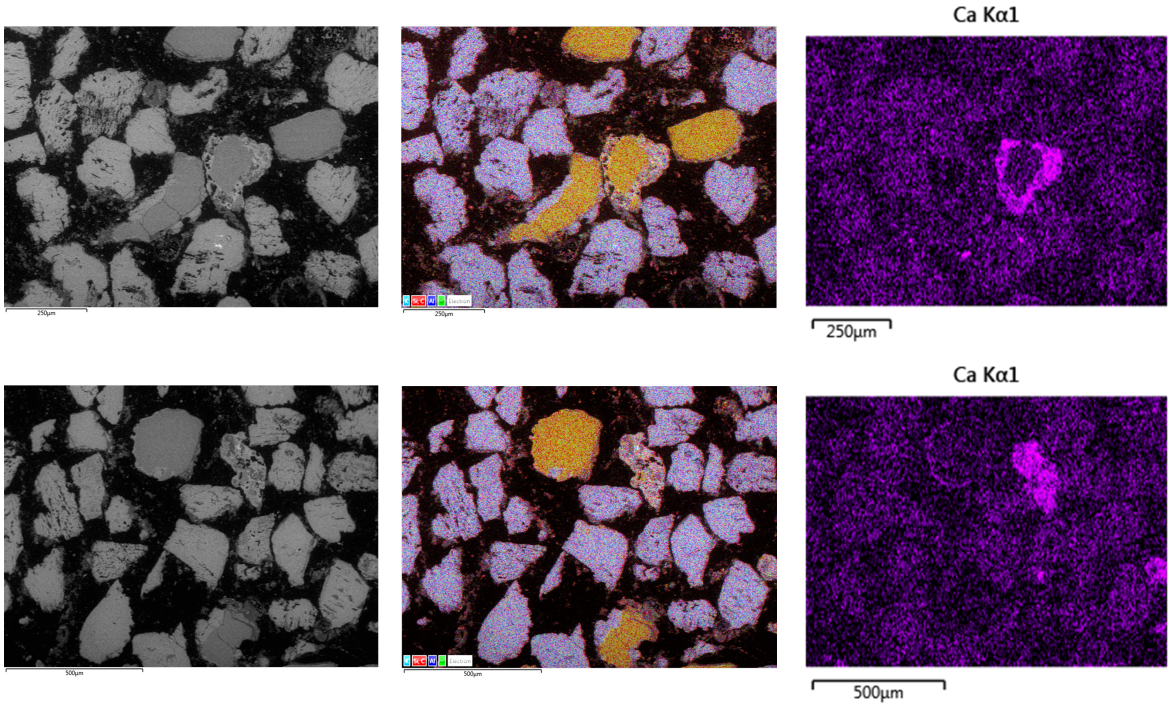

Figure 4.12: SEM images, layered element mappings and calcium (Ca) mappings of the bed sample after 4 hours into the combustion of Straw

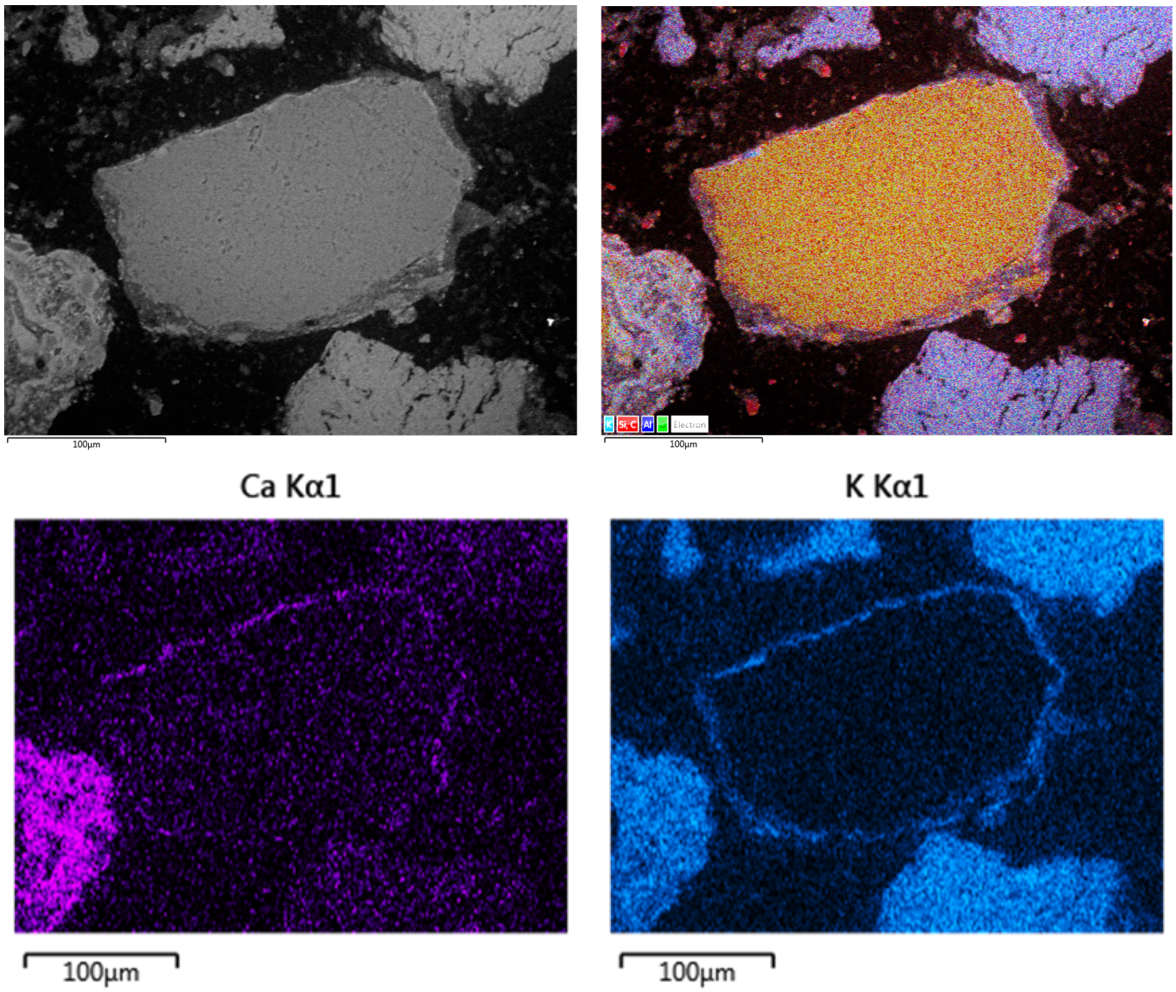

Figure 4.13: Quartz particle SEM image, layered element mapping, calcium (Ca) mapping and potassium (K) mapping of the bed sample after 4 hours into the combustion of Straw

5 Discussion

Layer formation during combustion of Straw

The SEM-EDS analysis for the Straw experiment (Figure 4.12) shows no layer formation on the feldspar particles after 4 hours of operation. The ash composition of Straw (Figure 4.2) shows the fuel rich in potassium (K) and silicon (Si) with little calcium (Ca) present. This leads to a total Ca/(K+Na) molar ratio of 0.34 for the Straw fuel pellets. The considerably less Ca in the biomass ash results in reduced interaction between calcium and the bed particle surface which leads to significantly diminished layer formation over time. This is in coherence with the findings for the 4-hour bed sample as no layer could be detected on the bed material. A comparison of the layer formation with a quartz particle in the same bed sample (Figure 4.13) shows that combustion of Straw with quartz as impurity in the K-feldspar bed material leads to the formation of K-layers with Ca diffusion, forming a Ca-rich layer on quartz over time. K-feldspar does not exhibit such behavior in the combustion of Straw as no layers were formed on the surface after 4 hours. The extended duration of the experiment with Straw compared to CLL was achieved by reducing the combustion temperature in the reactor. The reduced temperature lowered the fraction of molten ash in the fluidized bed causing the experiment to run longer compared to CLL. This measure was the logical conclusion following the early defluidization of the experiment with CLL after 2 hours.

Layer formation during combustion of Chicken Litter Low

As described in the SEM-EDS results for the combustion of CLL, the analysis did not reveal any signs of layer formation on the particles. The bed defluidized after approximately 2 hours which is too little time for any sufficient layer formation with the used fuel feedstock. The ash

composition of CLL (Figure 4.2) shows the high content of K, Ca, and Si in the biomass ash. K and Si form low-melting K-silicate ash particles/droplets that adhere to the surface of the bed materials leading to agglomeration of the fluidized-bed as described by Brus et al. (2005) and De Geyter et al. (2007). The combustion temperature of 780-800 ℃ probably led to an increased amount of molten ash fraction, especially the formed K-silicates, causing the fluidized bed to agglomerate faster. Additionally, the calcium content of CLL was too low to form sufficient amounts of high-temperature melting Ca-silicates that would have reduced the agglomeration problem.

Layer formation during combustion of Chicken Litter High

Initial layer formation on the feldspar bed particles was observed during operation until bed defluidization occured. Four bed samples were taken at 2 hours, 4 hours, 8 hours, and after defluidization (9h 32min). The 2-hour sample shows individual areas at the outline of the bed particles with discontinuous layers of calcium distributed on the particle surface. The 4-hour bed sample already reveals the beginning of continuous Ca-layers on the particle outline which is confirmed by the 8-hour bed sample, where a continuous qualitative layer is visible on the feldspar particles. In addition to that, phosphorus (P) was shown in the continuous layer formed on the 8-hour sample, but no magnesium (Mg) was detected within the elemental mappings. Phosphorus was also present in the calcium layer on the bed sample analyzed after defluidization.

The K-feldspar particle in the 2-hour sample (Figure 4.7) shows individual areas on the surface with higher amounts of calcium. This suggests low-melting ash particles sticking to the surface of the particle that contain calcium as well. No phosphorus, magnesium, or sulfur content was registered in the line scans or the element mappings of the individual Ca-rich areas. This could be attributed to the smaller amount of P in the total ash composition compared to K, Ca, and Mg together. Grimm et al. (2012b) pointed out that a limited amount of phosphorus implies a limited alkali retention effect. Phosphorus would form more stable compounds with Ca, Mg, and part of the available K, but the remaining K would be available to form low-melting K-silicates. The K-silicates would then adhere to individual bed particles

and cover only partially the bed particle surface. Other feldspar particles from the same 2 hour sample did not show individual areas with higher calcium content which makes it more plausible that low-melting ash particles would only stick to some bed particles. It would also be possible that low-melting K-silicates adhere to the particle surface and calcium started to diffuse into the molten phase. A comparison with the quartz particle extending into the picture on the bottom right corner shows a similar Ca-layer thickness as the individual areas on the K-feldspar. This does not suggest that the initial layer formation process is similar to quartz particles. It merely points out that the layer formation on K-feldspar may be influenced or delayed by low-melting K-silicates sticking to the surface when the phosphorus content in the biomass ash is low compared to the content of K, Ca, and Mg.

The 4-hour bed particle samples (Figure 4.8) show the first continuous Ca-layers on the surface of the K-feldspar particles in the calcium element mappings. The SEM images show a thin layer of ash attached along the particle circumference. The total ash composition of CLH (Figure 4.2) shows that the elements K, Ca, Mg, Si, P account for the majority in the biomass ash composition. Phosphorus and magnesium are not present in the ash layer on the particle. An explanation could be the same reason as described for the 2-hour bed sample. The increased amount of ash in the system could lead to further attachment of K-silicates on the particle surfaces with calcium-rich ash sticking to it and/or Ca diffusing into the molten phase. Interesting is the absence of the major ash elements P and Mg in the layer. After 4 hours, the total amount of phosphorus in the system could be too small to form noticable amounts of alkali orthophosphates (e.g. $CaKPO_4$, $KMgPO_4$) or pyrophosphates ($CaK_2P_2O_7$) that contain alkaline earth metals as described by Skoglund (2014).

The 8-hour bed particle samples (Figure 4.9) show continuous Ca-layers on their surface with individual particles (Figure 4.10) exibiting small amounts of phosphorus (P) in the layer as well. This leads to the suggestion that the content of phosphorus in the bed has reached a level after 8 hours of CLH combustion, where noticable P-containing ash fractions are formed. Based on the experiments by Skoglund (2014), it is very likely that a significant fraction of the bed ash now contains the main elements K, Ca, Mg, Si, and P, forming various stable and less stable phosphates in the bed ash. The formation and mixing of

high-temperature melting and low-temperature melting ash fractions can lead to further attachment of the Ca/K/Mg/P/Si-rich ash on the bed particle surfaces. Bed agglomeration was probably caused by an increased amount of low-melting ash fractions in the fluidized bed after more than 9 hours of operation.

The elemental composition of the used feldspar bed samples is different from the elemental composition of fresh feldspar (Figure 4.6). A decrease of potassium (K) and a similar reciprocal increase of calcium (Ca) in the used feldspar samples was noticable. The different amounts of Ca in the ash fractions had an influence on the elemental compositions of used K-feldspar particles in the combustion experiments. Straw ash with low Ca content caused only a small change, whereas CLH ash with a significantly higher Ca content caused a more significant change in the bed material composition. The K and Ca changes are accompanied by a decrease of Si and Al, and an increase of P and S. The described changes in elemental composition could be an indication for the suggested coupled substitution mechanisam for layer formation on K-feldspar particles. It has to be noted that the duration of the individual combustion experiments was different which influenced the elemental composition of the used feldspars to a certain extent as well.

The general formula for K-feldspar is $KAlSi_3O_8$. The substitution of K^{1+} with Ca^{2+} in the feldspar structure was characterized as unlikely to be a simple substitution mechanism due to the charge difference. Hence, other elements than K and Ca are probably involved in the mechanism to account for the generated charge difference. The other main ash-forming elements found in the elemental composition of the used K-feldspar particles after CLH combustion are Si, Al, P, S, Mg, and Fe. Therefore, the coupled substitution mechanism is likely to be influenced by one or more of those elements as well. The elements certainly affected by a substitution of K in the feldspar structure would be Si and Al, considering the general formula of K-feldspar. The coupled substitution mechanism of K with Ca probably causes local rearrangements of the K-feldspar structure, especially of the elements Al and Si. This structural rearrangement, coupled with the possible involvement of the elements P, S, Mg, and/or Fe in the mechanism, could cause marginal expulsion of Al and Si as well. Reduced amounts of Al and Si were found in the elemental composition of the used feldspars, es-

pecially for CLH combustion, and the elements P, S, Mg, and Fe were found in the used feldspar composition. It has to be noted that only one XRF analysis was carried out for the sample and that multiple analyses would probably lead to a more accurate representation of the actual elemental composition of used feldspars. Nevertheless, the identified elements in the elemental composition of used K-feldspar suggest some form of ash-related layer formation process with Ca as the important element for the coupled substitution mechanism.

Line scans were conducted to determine the quantitative composition of the qualitative layers observed on the element mappings. The majority of the scan results showed single Ca peaks in the areas were qualitative layers were observed. Only a few line scans determined the Ca content over a length of 1.0-3.0 µm. Hence, the determination of the layer thickness and the elemental distribution was limited with the used K-feldspar sample. This shows that layer formation on the bed particles was in the initial stage after about 8 hours during combustion of CLH. The formation of more advanced layers would have enabled a better determination of the thickness and elemental distribution. Longer experiments would have probably facilitated further layer growth which would have given further insights into initial layer formation on K-feldspar.

6 Conclusions

The three combustion experiments showed that the biomass ash composition had a significant influence on bed agglomeration of the fluidized bed and the layer formation on the K-feldspar particles. Chicken Litter Low and Straw provided unfavorable ash compositions for layer formation on K-feldspar until defluidization occured. Among the three different ash compositions, only the biomass ash of Chicken Litter High showed beginning layer formation on the bed particles within the first hours of operation. The ash of CLH was characterized with increased amounts of Ca, Mg, P, and S. This showed that the relative amounts of certain main ash-forming elements in the fuels such as K, Ca, Mg, Si, P, and S are crucial for the layer formation. The evaluation of individual and layered element mappings led to the conclusion that the layer formation process on K-feldspar could be ash-related.

Future experiments should implement fuel blends with even higher content of Ca, Mg, P, and S. This should facilitate the formation of more stable alkali orthophosphates and pyrophosphates leading to a longer duration of the experiments as the formation of low-melting K-silicates should be reduced. Based on the results of this thesis, a longer combustion time together with higher amounts of Ca in the ash should improve the layer formation on K-feldspar significantly. The analysis should then be focused on the elemental composition of the bed particle surface to detect possible differences compared to the fresh K-feldspar particles. Quantitative line scans across further advanced layers could then help to determine the elemental distribution and provide better insights into the coupled substitution mechanism. The elemental distribution of the layers over time could help to identify the elements involved in the coupled substitution mechanism apart from potassium and calcium.

Bibliography

Basu, P. (2010). *Biomass gasification and pyrolysis: practical design and theory*. Academic press.

Berdugo Vilches, T., Lind, F., Rydén, M., & Thunman, H. (2017). Experience of more than 1000 h of operation with oxygen carriers and solid biomass at large scale. *Applied Energy*, 190, 1174–1183.

Berdugo Vilches, T., Marinkovic, J., Seemann, M., & Thunman, H. (2016). Comparing Active Bed Materials in a Dual Fluidized Bed Biomass Gasifier: Olivine, Bauxite, Quartz-Sand, and Ilmenite. *Energy & Fuels*, 30(6), 4848–4857.

Berguerand, N., Marinkovic, J., Berdugo Vilches, T., & Thunman, H. (2016). Use of alkali-feldspar as bed material for upgrading a biomass-derived producer gas from a gasifier. *Chemical Engineering Journal*, 295, 80–91.

Boström, D., Skoglund, N., Grimm, A., Boman, C., Öhman, M., Broström, M., & Backman, R. (2012). Ash Transformation Chemistry during Combustion of Biomass. *Energy & Fuels*, 26(1), 85–93.

Bridgewater, A. V., Hofbauer, H., & Van Loo, S. (2009). *Thermal Biomass Conversion*. CPL Press.

Brus, E., Öhman, M., & Nordin, A. (2005). Mechanisms of bed agglomeration during fluidized-bed combustion of biomass fuels. *Energy & Fuels*, 19(3), 825–832.

Brus, E., Öhman, M., Nordin, A., Boström, D., Hedman, H., & Eklund, A. (2004). Bed Agglomeration Characteristics of Biomass Fuels Using Blast-Furnace Slag as Bed Material. *Energy & Fuels*, 18(4), 1187–1193.

Brus, E., Öhman, M., Nordin, A., Skrifvars, B., & Backman, R. (2003). Bed material consumption in biomass fired fluidised bed biolers due to risk for bed agglomeration: coating formation and possibilities for regeneration. *Industrial Combustion*, (2), 1–12.

Christodoulou, C., Grimekis, D., Panopoulos, K. D., Pachatouridou, E. P., Iliopoulou, E. F., & Kakaras, E. (2014). Comparing calcined and un-treated olivine as bed materials for tar reduction in fluidized bed gasification. *Fuel Processing Technology*, 124, 275–285.

Corcoran, A., Marinkovic, J., Lind, F., Thunman, H., Knutsson, P., & Seemann, M. (2014). Ash Properties of Ilmenite Used as Bed Material for Combustion of Biomass in a Circulating Fluidized Bed Boiler. *Energy & Fuels*, 28(12), 7672–7679.

Davidsson, K. O., Åmand, L. E., Steenari, B. M., Elled, A. L., Eskilsson, D., & Leckner, B. (2008). Countermeasures against alkali-related problems during combustion of biomass in a circulating fluidized bed boiler. *Chemical Engineering Science*, 63(21), 5314–5329.

De Geyter, S., Öhman, M., Boström, D., Eriksson, M., & Nordin, A. (2007). Effects of non-quartz minerals in natural bed sand on agglomeration characteristics during fluidized bed combustion of biomass fuels. *Energy & Fuels*, 21(5), 2663–2668.

Delgado, J., Aznar, M. P., & Corella, J. (1997). Biomass gasification with steam in fluidized bed: Effectiveness of CaO, MgO, and CaO-MgO for hot raw gas cleaning. *Industrial & Engineering Chemistry Research*, 36(5), 1535–1543.

ECN (2017). Phyllis2 database for biomass and waste. Energy research Centre of the Netherlands.

Göransson, K., Söderlind, U., Engstrand, P., & Zhang, W. (2015). An experimental study on catalytic bed materials in a biomass dual fluidised bed gasifier. *Renewable Energy*, 81, 251–261.

Greenwood, N. N. & Earnshaw, A. (1995). 9 - Silicon. In N. GREENWOOD & A. EARNSHAW (Eds.), *Chemistry of the Elements* (pp. 328 – 366). Oxford [u.a.]: Butterworth-Heinemann, reprinted edition.

Grimm, A., Boström, D., Lindberg, T., Fredriksson, A., & Öhman, M. (2011). Bed agglomeration characteristics during fluidized olivine bed combustion of typical biofuels. In *European Biomass Conference & Exhibition* (pp. 1345–1350).: ETA-Renewable Energies.

Grimm, A., Öhman, M., Lindberg, T., Fredriksson, A., & Boström, D. (2012a). Bed agglomeration characteristics in fluidized-bed combustion of biomass fuels using olivine as bed material. *Energy & Fuels*, 26(7), 4550–4559.

Grimm, A., Skoglund, N., Boström, D., Boman, C., & Öhman, M. (2012b). Influence of phosphorus on alkali distribution during combustion of logging residues and wheat straw in a bench-scale fluidized bed. *Energy & Fuels*, 26(5), 3012–3023.

He, H., Boström, D., & Öhman, M. (2014). Time dependence of bed particle layer formation in fluidized quartz bed combustion of wood-derived fuels. *Energy & Fuels*, 28(6), 3841–3848.

He, H., Ji, X., Boström, D., Backman, R., & Öhman, M. (2016). Mechanism of quartz bed particle layer formation in fluidized bed combustion of wood-derived fuels. *Energy & Fuels*, 30(3), 2227–2232.

He, H., Skoglund, N., & Öhman, M. (2017). Time-Dependent Crack Layer Formation in Quartz Bed Particles during Fluidized Bed Combustion of Woody Biomass. *Energy & Fuels*, 31(2), 1672–1677.

Öhman, M. & Nordin, A. (1998). A new method for quantification of fluidized bed agglomeration tendencies: A sensitivity analysis. *Energy & Fuels*, 12(1), 90–94.

Öhman, M. & Nordin, A. (2000). The role of kaolin in prevention of bed agglomeration during fluidized bed combustion of biomass fuels. *Energy & Fuels*, 14(3), 618–624.

Öhman, M., Pommer, L., & Nordin, A. (2005). Bed Agglomeration Characteristics and Mechanisms during Gasification and Combustion of Biomass Fuels. *Energy & Fuels*, 19(4), 1742–1748.

Kaknics, J., Michel, R., & Poirier, J. (2016). Miscanthus ash transformation and interaction with bed materials at high temperature. *Fuel Processing Technology*, 141, Part 2, 178–184.

Kaltschmitt, M., Hartmann, H., & Hofbauer, H. (2009). *Energie aus Biomasse; Grundlagen, Techniken und Verfahren*. Berlin, Heidelberg: Springer Berlin Heidelberg, 2nd edition.

Kirnbauer, F. & Hofbauer, H. (2011). Investigations on bed material changes in a dual fluidized bed steam gasification plant in güssing, austria. *Energy & Fuels*, 25(8), 3793–3798.

Kirnbauer, F. & Hofbauer, H. (2013). The mechanism of bed material coating in dual fluidized bed biomass steam gasification plants and its impact on plant optimization. *Powder Technology*, 245, 94–104.

Kirnbauer, F., Wilk, V., Kitzler, H., Kern, S., & Hofbauer, H. (2012). The positive effects of bed material coating on tar reduction in a dual fluidized bed gasifier. *Fuel*, 95, 553–562.

Källen, M., Rydén, M., & Lind, F. (2015). *Improved Performance in Fluidised Bed Combustion by the Use of Manganese Ore as Active Bed Material*. 22nd International Conference on Fluidized Bed Conversion, 14-17 June 2015, Turku.

Knutsson, P., Schwebel, G., Steenari, B.-M., & Leion, H. (2014). *Effect of bed materials mixing on the observed bed sintering*, volume s. 655-660. 11th International Conference on Fluidized Bed Technology, CFB 2014; Beijing; China; 14 May 2014 through 17 May 2014.

Kuba, M. (2016). *Interactions between bed material and biomass ash in dual fluid bed gasification*. PhD thesis, Vienna University of Technology. PhD thesis, Technische Universität Wien, 2016.

Kuba, M., Havlik, F., Kirnbauer, F., & Hofbauer, H. (2016a). Influence of bed material coatings on the water-gas-shift reaction and steam reforming of toluene as tar model compound of biomass gasification. *Biomass and Bioenergy*, 89, 40–49.

Kuba, M., He, H., Kirnbauer, F., Boström, D., Öhman, M., & Hofbauer, H. (2015). Deposit build-up and ash behavior in dual fluid bed steam gasification of logging residues in an industrial power plant. *Fuel Processing Technology*, 139, 33–41.

Kuba, M., He, H., Kirnbauer, F., Skoglund, N., Boström, D., Öhman, M., & Hofbauer, H. (2016b). Mechanism of layer formation on olivine bed particles in industrial-scale dual fluid bed gasification of wood. *Energy & Fuels*, 30(9), 7410–7418.

Kuba, M., He, H., Kirnbauer, F., Skoglund, N., Boström, D., Öhman, M., & Hofbauer, H. (2016c). Thermal Stability of Bed Particle Layers on Naturally Occurring Minerals from Dual Fluid Bed Gasification of Woody Biomass. *Energy & Fuels*, 30(10), 8277–8285.

Kuba, M., Kirnbauer, F., & Hofbauer, H. (2016d). Influence of coated olivine on the conversion of intermediate products from decomposition of biomass tars during gasification. *Biomass Conversion and Biorefinery*, (pp. 1–11).

Lackner, M. H. (2010). *Handbook of Combustion: Solid fuels*. Weinheim: Wiley-VCH.

Larsson, A., Israelsson, M., Lind, F., Seemann, M., & Thunman, H. (2014). Using ilmenite to reduce the tar yield in a dual fluidized bed gasification system. *Energy & Fuels*, 28(4), 2632–2644.

Ma, T., Fan, C., Hao, L., Li, S., Song, W., & Lin, W. (2016). Biomass-Ash-Induced Agglomeration in a Fluidized Bed. Part 1: Experimental Study on the Effects of a Gas Atmosphere. *Energy & Fuels*, 30(8), 6395–6404.

Mac an Bhaird, S. T., Walsh, E., Hemmingway, P., Maglinao, A. L., Capareda, S. C., & McDonnell, K. P. (2014). Analysis of bed agglomeration during gasification of wheat straw in a bubbling fluidised bed gasifier using mullite as bed material. *Powder Technology*, 254, 448–459.

Marinkovic, J., Berguerand, N., Lind, F., Seemann, M., & Thunman, H. (2015a). Using a manganese ore as catalyst for upgrading biomass derived gas. *Biomass Conversion and Biorefinery*, 5(1), 75–83.

Marinkovic, J., Seemann, M., Schwebel, G. L., & Thunman, H. (2016). Impact of biomass ash–bauxite bed interactions on an indirect biomass gasifier. *Energy & Fuels*, 30(5), 4044–4052.

Marinkovic, J., Thunman, H., Knutsson, P., & Seemann, M. (2015b). Characteristics of olivine as a bed material in an indirect biomass gasifier. *Chemical Engineering Journal*, 279, 555–566.

Moradian, F., Tchoffor, P. A., Davidsson, K. O., Pettersson, A., & Backman, R. (2016). Thermodynamic equilibrium prediction of bed agglomeration tendency in dual fluidized-bed gasification of forest residues. *Fuel Processing Technology*, 154, 82–90.

Nikolaisen, L. S. & Jensen, P. D. (2013). *3 - Biomass feedstocks: categorisation and preparation for combustion and gasification A2 - Rosendahl, Lasse*, (pp. 36–57). Woodhead Publishing.

Nordgreen, T., Liliedahl, T., & Sjöström, K. (2006a). Elemental iron as a tar breakdown catalyst in conjunction with atmospheric fluidized bed gasification of biomass: A thermodynamic study. *Energy & Fuels*, 20(3), 890–895.

Nordgreen, T., Liliedahl, T., & Sjöström, K. (2006b). Metallic iron as a tar breakdown catalyst related to atmospheric, fluidised bed gasification of biomass. *Fuel*, 85(5–6), 689–694.

Rosendahl, L. e. (4 April 2013). *Biomass Combustion Science, Technology and Engineering*. Woodhead Publishing Series in Energy. Elsevier Science.

Rydén, M., Hanning, M., Corcoran, A., & Lind, F. (2016). Oxygen carrier aided combustion (ocac) of wood chips in a semi-commercial circulating fluidized bed boiler using manganese ore as bed material. *Applied Sciences*, 6(11), 347.

Serrano, D., Kwapinska, M., Horvat, A., Sánchez-Delgado, S., & Leahy, J. J. (2016). Cynara cardunculus l. gasification in a bubbling fluidized bed: The effect of magnesite and olivine on product gas, tar and gasification performance. *Fuel*, 173, 247–259.

Serrano, D., Sánchez-Delgado, S., & Horvat, A. (2017). Effect of sepiolite bed material on gas composition and tar mitigation during c. cardunculus l. gasification. *Chemical Engineering Journal*, 317, 1037–1046.

Serrano, D., Sánchez-Delgado, S., Sobrino, C., & Marugán-Cruz, C. (2015). Defluidization and agglomeration of a fluidized bed reactor during cynara cardunculus l. gasification using sepiolite as a bed material. *Fuel Processing Technology*, 131, 338–347.

Skoglund, N. (2014). *Ash chemistry and fuel design focusing on combustion of phosphorus-rich biomass*. PhD thesis, Umeå University, Department of Applied Physics and Electronics.

Skoglund, N., Grimm, A., Öhman, M., & Boström, D. (2013). Effects on ash chemistry when co-firing municipal sewage sludge and wheat straw in a fluidized bed: Influence on the ash chemistry by fuel mixing. *Energy & Fuels*, 27(10), 5725–5732.

Valmari, T., Lind, T. M., Kauppinen, E. I., Sfiris, G., Nilsson, K., & Maenhaut, W. (1999). Field study on ash behavior during circulating fluidized-bed combustion of biomass. 1. ash formation. *Energy & Fuels*, 13(2), 379–389.

van Loo, S. & Koppejan, J. (2012). *The handbook of biomass combustion & co-firing; Biomass combustion & co-firing*.

Vassilev, S. V., Baxter, D., Andersen, L. K., & Vassileva, C. G. (2010). An overview of the chemical composition of biomass. *Fuel*, 89(5), 913–933.

Visser, H. J. M., Kiel, J., & Veringa, H. (2004). *The influence of fuel composition on agglomeration behaviour in fluidised-bed combustion*. Energy research Centre of the Netherlands ECN Delft.

Zevenhoven-Onderwater, M., Backman, R., Skrifvars, B. J., & Hupa, M. (2001). The ash chemistry in fluidised bed gasification of biomass fuels. part i: predicting the chemistry of melting ashes and ash-bed material interaction. *Fuel*, 80(10), 1489–1502.